1997

The calculation of cyclic strain ranges at local discontinuites of a structure in low cycle fatigue using FEM

Ingyu Park
Lehigh University

Park, Ingyu

The Calculation of Cyclic Strain Ranges at Local Discontinuities of a Structure in Low Cycle Fatigue...

June 1, 1997

The Calculation of Cyclic Strain Ranges at Local Discontinuities of A Structure in Low Cycle Fatigue Using FEM

by

Ingyu Park

A Thesis

Presented to the Graduate and Research Committee

of Lehigh University

in Candidacy for the Degree of

Master of Science

in

Mechanical Engineering

Lehigh University

May, 1997

This thesis is accepted and approved in partial fulfillment of the requirement for the Master of Science.

April 21, 1997

date

Professor Arturs Kalnins

Thesis Advisor

Professor Charles R. Smith

Chairperson of Department

To my parents, the late Il-Sung Park and Soon-Ja Shin

my wife, Young-Ja

and my children, Soo-Jin and Sung-Hyun

ACKNOWLEDGMENTS

I would like to express my sincere thanks to Prof. Arturs Kalnins who has helped me as my thesis advisor throughout this work, and Prof. Dean P. Updike who has helped me as my thesis consultor. They instructed me and suggested many things for my thesis with hearty kindness until this work has been completed. Also, I would like to appreciate the financial support from Hyundai Motor Company while I have been staying at Lehigh and thank to Mr. Sung-Soo Jung, Young-Woo Lee, Jin-Hyun Kim, and Korean Students in Lehigh University.

And, I should thank my lovely wife who has spent many hard days with our children and has assisted me with sincerity during my study, and my lovely children, my hope, who have missed many pleasant hours with their father in Lehigh.

Finally, I greatly appreciate my mother spending too many lonely days and waiting for me in Korea after sending her only son to study abroad. I willingly attribute this work to them.

TABLE OF CONTENTS

LIST OF TABLES

LIST OF FIGURES

NOMENCLATURE

a	Radius of the circular hole
A	Section area
b	Edge length of the quarter-plate
D	Diameter of a cylinder
e	Nominal strain
E	Young's modulus
E11, E22, E12	Strain components in ABAQUS
E_{eq}	Equivalent elastic strain
E_{eq}^{p}	Equivalent plastic strain
E_{Range}	Cycled equivalent strain range
G	Shear modulus
h	Width of plate
K_{ε}, ECF	Strain Concentration Factor
K_{tg}, K_{tn}, K_t, SCF	Stress Concentration Factor
L	Radius of sphere
M_0	Applied edge moment
M_p	Plastic moment
M_θ	Circumferential bending moment
M_φ, M_θ	Bending moments in a shell per unit length of meridional section and a section perpendicular to meridian, respectively
N_φ, N_θ	Membrane forces per unit length of principal normal sections of a shell
p	Uniform pressure
P_{sk}	Shakedown pressure
Q	Transverse shear resultant force
r	Radius

r_0	Radius of a parallel circle on a torus
r_a	Radius of a circle in torus or radius of a cylinder and a sphere
S_0	Applied uniaxial edge traction far away from the hole
S11, S22, S12	Stress components in ABAQUS
S'	Equivalent stress difference intensities
t	Thickness of a plate
t_n	Thickness of a nozzle
u_x, u_y, u_z	Components of displacement
$w_{,x}$, $w_{,y}$	Derivatives of deflection with respect to x and y
Y	Yield strength
β_x, β_y	Rotation angles of the normal of the reference plane
ε	Total strain
ε_1, ε_2, ε_3	Principal strains
ε_x, ε_y, ε_z	Normal strain components
ε_{xy}, ε_{yz}, ε_{zx}	Shear strain components
ε_e	Elastic strain
ε_p	Plastic strain
ϕ_x, ϕ_y, ϕ_z	Components of rotation
γ_{zx}, γ_{yz}	Transverse shear strains
ν	Poisson's ratio
φ, θ	Angle
σ	Stress
σ_1 , σ_2 , σ_3	Principal stresses
σ_{alt}	Alternating stress being cycled
σ_{max}	Maximum stress
σ_{nom}	Nominal stress
σ_0	Applied stress, far-away from a hole
σ_x , σ_y , σ_z	Normal stress components parallel to x, y, and z axes

σ_r , σ_θ	Radial and tangential normal stresses in Polar Coordinates
τ_{xy} , τ_{yz} , τ_{xz}	Shearing stress components in rectangular coordinates
$\tau_{r\theta}$	Shearing stress in polar coordinates

ABSTRACT

Material failure in the proximity of holes, notches, nozzles, and non-integral attachments is the main reason of failure of a structure under repeated cycles of loading and unloading. Thus, it is important to be able to estimate the maximum strain range being cycled in order to determine the number of cycles to failure of a structure. In this thesis, the effect of a small-diameter nozzle in the knuckle of a torispherical head on the elastic stress concentration factor and the strain range produced by cyclic internal pressure is investigated. The purpose of this thesis is to estimate the maximum strain range being cycled in the head at the nozzle and the shakedown pressure. At first, as a simple model, the geometry of a square plate with a hole and a nozzle under in-plane and bending loads, is considered. From this simple example, it is found that the use of an elastic-plastic large deflection analysis is a more effective approach for an economical design of a structure than an elastic analysis. Also, for this model, the most highly stressed location is found when the nozzle is attached. Then, the stress concentration factors are obtained for a number of torispherical head and nozzle wall thicknesses. It is determined that, depending on the head and nozzle wall thicknesses, these factors are between 1.4 and 2.1. The maximum strain range being cycled in the head at the nozzle is calculated by elastic analysis and the shakedown pressure is estimated from the maximum von Mises stress intensity and the yield strength of a material.

Chapter 1

INTRODUCTION

To effectively and economically design any structure, countless design criteria, such as elastic and plastic analysis, NVH(Noise Vibration Hardness), CAD(Computer Aided Design), and impact analysis, should be performed. Recently, thanks to the rapid development of powerful supercomputer systems and diverse software, it is feasible to perform numerous simulation analyses. In this thesis, most of calculations are performed employing a computer with commercial software. In addition,a special code, KSHEL, developed for elastic-plastic analysis by Updike and Kalnins (1991) is also used for simulations.

For structural failure caused by low cycle fatigue, it is important to estimate the maximum strain range at a location where local discontinuities exist. Elastic analysis is performed to determine the maximum stress point of the structure, prior to performing a plastic analysis; a geometrically non-linear, elastic-perfectly plastic algorithm is employed to estimate the maximum strain range. If a local discontinuity exists in the structure, the maximum stress will be found in the proximity. As an example, for a pressure vessel consisting of a torispherical head (i.e. the spherical dome), a toroidal knuckle, and a cylindrical body, local discontinuities can exist as nozzles in the knuckle. In order to calculate elastic and plastic solutions for such a complex geometry, the stress and strain concentration can be examined for a simplified model such as a square plate with a hole

subjected to in-plane tension and out-of-plane bending. Then, the results from the simple model can be applied to the analysis of the torispherical head as a complex geometry.

1.1 OBJECTIVE

Fatigue failure is defined as the fracture of a material caused by repetitive action of a load. According to B. F. Langer[1], there are two types of fracture characteristics of a material; the transgranular crack produced by fatigue and the intergranular crack which is stress rupture failure. These are employed to investigate the failures to determine whether the cause of failure is a steady or a repetitive type of loading. In this thesis, fracture produced by fatigue due to a repetitive loading is examined.

Generally, there is high cycle fatigue governed by the endurance limit of a structure and low cycle fatigue governed by the total strain range applied to the structure. In low cycle fatigue, bounded from a lower limit of a few hundred cycles to an upper limit of a few hundred thousand cycles, stress can not be used as a variable to analyze the fatigue behavior of a material since the applied stresses usually exceeds the yield strength of the material and plastic yielding produces redistribution of the stresses in the specimen. Langer [1,13] uses the strain range as a controlled variable in his experiments to achieve more reliable results; when the stress at the root of a notch exceeds the yield strength, it was found that the strain concentration factor increases with decrease in stress concentration factor. These results were calculated employing plastic analysis and verified experimentally with initial loading only, but cyclic loading was not considered..

The objective of this thesis is to investigate low cycle fatigue with applied stress under cyclic loading and to estimate the maximum strain range being cycled for given geometries when shakedown is achieved. The effectiveness of employing an elastic-plastic, large deflection analysis instead of employing simple elastic analysis to predict the lifetime of a material will be examined. The well-known commercial finite-element software, ABAQUS, is employed to determine the results from finite-element models of structures. The results from this study can be used to estimate the low-cycle fatigue life of a torispherical head when subjected to cyclic pressure.

1.2 PREVIOUS STUDIES

1.2.1 Stress and Strain Concentration Factors (K_t, K_ε)

If a local discontinuity exists in a structure, such as a hole, a nozzle, or an attachment, the stress that is found in the region near the discontinuity is significantly greater than far-field stress of regions distant from the discontinuity. The stress concentration factor (SCF) can be calculated numerically if the maximum stress and far-field stress are known. Theoretically, there are two types of stress concentration factors that can be calculated [2]

$$K_{tg} = \frac{\sigma_{max}}{\sigma_0} \quad \text{----------} \quad (1\text{-}1)$$

where K_{tg} = stress concentration factor based on gross stress

σ_{max} = maximum stress, at edge of the hole

σ_0 = applied stress, far away from the hole

and

$$K_{tn} = \frac{\sigma_{max}}{\sigma_{nom}} \quad \text{---------- (1-2)}$$

where K_{tn} = stress concentration factor based on net(nominal) stress

σ_{nom} = nominal(net) stress = $\sigma_0/(1-2a/h)$

where a = radius of the circular hole

h = width of plate

but, since the width of a plate is assumed to be much greater than the hole radius, the ratio, $2a/h$ tends to zero; equation (1-1) will be identical to equation (1-2). Therefore, equation (1-1) will be employed to calculate the stress concentration factor.

For the case of a single circular hole in an infinite plate in uniaxial tension, Kirsch[3] states that the stress concentration factor is three, based on the theory of elasticity:

$$\sigma_r = \frac{S_0}{2}(1-\frac{a^2}{r^2}) + \frac{S_0}{2}(1+\frac{3a^4}{r^4}-\frac{4a^2}{r^2})\cos 2\theta$$

$$\sigma_\theta = \frac{S_0}{2}(1+\frac{a^2}{r^2}) - \frac{S_0}{2}(1+\frac{3a^4}{r^4})\cos 2\theta \quad \text{---------- (1-3)}$$

$$\tau_{r\theta} = -\frac{S_0}{2}(1-\frac{3a^4}{r^4}+\frac{2a^2}{r^2})\sin 2\theta$$

where σ_r, σ_θ = radial and tangential normal stresses in polar coordinates

S_0 = the applied uniaxial edge traction far away from the hole

$\tau_{r\theta}$ = shearing stress in polar coordinates

r = radius

At the edge of the hole, $r = a$, equation (1-3) can then be expressed as [4]:

$$\sigma_r = \tau_{r\theta} = 0, \qquad \sigma_\theta = S_0(1-2\cos 2\theta) \quad \text{----------} \quad (1\text{-}4)$$

which implies that the stress is independent of the thickness of a plate. The stress distribution along the edge, $\overline{AB}$ [Figure 1.1], perpendicular to the direction of the tension is calculated employing ABAQUS and is shown in Figure 1.2. The stress plotted in Figure 1.2 is the von Mises stress intensity or the equivalent stress. As shown in Figure 1.2, the maximum equivalent stress is found on the edge of the hole when $\theta = \frac{\pi}{2}$, where the stress is three times as large as that of the applied traction far from the hole. By using equation (1-4), it is confirmed that the stress concentration factor is three when $\theta = \frac{\pi}{2}$.

When out-of-plane bending is applied to the edge, instead of an in-plane force, Reissner [2] calculated the stress concentration factor as a function of $2a/h$; if the length of the edge of the plate is much greater than the radius of the hole, $2a/h \to 0$, and the stress concentration factor approaches three as $2a/h \to \infty$:

$$K_t = \frac{5+3\nu}{3+\nu} \quad \text{----------} \quad (1\text{-}5)$$

for $\nu = 0.3$, $K_t = 1.788$.

The elastic circumferential bending moment distribution around the hole can be expressed as [4]:

$$M_\theta = M_0[1 - \frac{2(1+\nu)}{3+\nu}\cos 2\theta] \quad \text{----------} \quad (1\text{-}6)$$

where M_0 = the applied edge moment, far away from the hole

The stress concentration factor under an applied moment can also be calculated as a function of $2r/t$ [5]:

$$K_t = 1.79 + \frac{0.25}{0.39 + (2r/t)} + \frac{0.81}{1 + (2r/t)^2} - \frac{0.26}{1 + (2r/t)^3} \quad \text{----------(1-7)}$$

where t = thickness of a plate

The results from the ABAQUS finite element code and from equation (1-7) are listed in Table 1.1 and shown in Figure 1.3; it is clear that the solution determined from the ABAQUS code confirms approximately the theoretical solution obtained from equation (1-7).

The elastic strain concentration factor (ECF), K_ε, represents the ratio of maximum strain at the hole to the nominal strain and is defined as the elastic stress divided by the Young's modulus. When the applied forces are uniaxial, the stress and strain concentration factor is the same in the elastic region. When the local stress at the edge of the hole exceeds the yield strength, the local stress is less than $K_t S_0$. Then, the stress concentration factor, K_t, can no longer be employed to calculate $\sigma = K_t S_0$ since the strain concentration factor is increased while the stress concentration factor is decreased, in a plastic region, as shown in Figure 1.4 [1]. Therefore, the ECF in a plastic region should be calculated using the following equation [6]:

$$K_\varepsilon = \frac{\varepsilon}{e} \quad \text{----------(1.8)}$$

where K_ε = strain concentration factor

ε = total strain at the side of the hole ($= \varepsilon_e + \varepsilon_p$)

e = nominal strain (applied stress divided by Young's modulus)

The total strain is the sum of the strain due to elastic behavior and plastic deformation. Denoting the elastic strain by ε_e and the plastic strain by ε_p, the total strain is calculated from

$$\varepsilon = \varepsilon_e + \varepsilon_p \quad \text{----------(1-9)}$$

The strain concentration factor in a plastic region under cyclic loading, will be discussed in the following sections.

1.2.2 Tresca and von Mises Theories

The two experimentally verified, yield criterion theories are the maximum shear-stress theory of Tresca and the maximum-distortion-energy theory of von Mises. The yield criterion is employed to determine if plastic deformation has taken place or if it is even possible to occur plastic deformation. When a material is isotropic, plastic yielding depends on the magnitudes of the three principal stresses, σ_1, σ_2, and σ_3. Assume that the magnitude of the three principal stresses are related as $\sigma_1 > \sigma_2 > \sigma_3$. Then the stress intensity, S, can be expressed as [1,9,10]

Tresca yielding criterion $S = \sigma_1 - \sigma_3$ ----------(1-10)

Von Mises yielding criterion $S = \sqrt{\frac{1}{2}[(\sigma_1 - \sigma_2)^2 + (\sigma_2 - \sigma_3)^2 + (\sigma_3 - \sigma_1)^2]}$ --(1-11)

where von Mises criterion is more accurate while Tresca's criterion is more conservative, which was confirmed from a torsion test [7]. A comparison of the two criteria is shown in Figure 1.5, assuming $\sigma_3 = 0$. When the stress is uniaxial, the two theories coincide at the same point on the σ_1 or the σ_2 axes and when the stress is biaxial, the average difference between the theories is 8-10 % with the maximum difference never exceeding 15.5 %.

Langer [1,8] recommends the use of the Tresca theory as the failure criterion for examining fatigue problems involving stress reversals due to the fact that von Mises theory has the practical disadvantage that the stress intensity has no direction or sign due to the square root sign in equation (1-11). However, it seems that he did not apply the range of stress to von Mises theory while applying it to the Tresca theory.

To calculate the allowable alternating stresses and to estimate the number of cycles, the ranges of stress and strain are important parameters for fatigue failure analysis. If the directions of the principal stresses at a point being considered, change during the stress cycle, the following procedure can be used to calculate the stress intensities with respect to time t and t_i [14].

(1) For the complete stress cycle, the values of the six stress components versus time t are: $\sigma_x(t), \sigma_y(t), \sigma_z(t), \tau_{xy}(t), \tau_{yz}(t), \tau_{xz}(t)$

(2) At a point in time, when the conditions are one of the extremes for the cycle (i.e. magnitude is either maximum or minimum), the values of the six stress components at this time with the subscript i are: $\sigma_x(t_i), \sigma_y(t_i), \sigma_z(t_i), \tau_{xy}(t_i), \tau_{yz}(t_i), \tau_{xz}(t_i)$

In most cases, it is possible to choose at least one time during the cycle when the conditions are known to be an extreme, but in some cases, it may be necessary to try different points in time to find the one which results in the largest value of alternating stress intensity.

(3) Subtract each of the six stress components in (2) from (1).

$$\sigma_x' = \sigma_x(t) - \sigma_x(t_i) \quad \sigma_y' = \sigma_y(t) - \sigma_y(t_i) \quad \sigma_z' = \sigma_z(t) - \sigma_z(t_i)$$

$$\tau_{xy}' = \tau_{xy}(t) - \tau_{xy}(t_i) \quad \tau_{yz}' = \tau_{yz}(t) - \tau_{yz}(t_i) \quad \tau_{xz}' = \tau_{xz}(t) - \tau_{xz}(t_i) \quad \text{--(1-12)}$$

(4) Calculate the principal stresses σ_1', σ_2', and σ_3' derived from the new six stress components in equation (1-12) by using the following cubic equation in J:

$$J^3 - (\sigma_x' + \sigma_y' + \sigma_z')J^2 + (\sigma_x'\sigma_y' + \sigma_y'\sigma_z' + \sigma_z'\sigma_x' - \tau_{xy}'^2 - \tau_{yz}'^2 - \tau_{xz}'^2)J$$

$$-(\sigma_x'\sigma_y'\sigma_z' + 2\tau_{xy}'\tau_{yz}'\tau_{xz}' - \sigma_x'\tau_{yz}'^2 - \sigma_y'\tau_{xz}'^2 - \sigma_z'\tau_{xy}'^2) = 0 \quad \text{-------(1-13)}$$

The three roots of this equation are the values of the three principal stresses σ_1', σ_2', and σ_3'.

By employing the three principal stresses derived from the above procedure, the equivalent stress difference intensities, S', for fatigue failure of a ductile material can be calculated based on Tresca *and* von Mises theories:

Tresca theory $$S' = \max\left(\left|\sigma_1' - \sigma_2'\right|, \left|\sigma_2' - \sigma_3'\right|, \left|\sigma_3' - \sigma_1'\right|\right) \quad \text{----------(1-14)}$$

von Mises theory $$S' = \sqrt{\frac{1}{2}[(\sigma_1' - \sigma_2')^2 + (\sigma_2' - \sigma_3')^2 + (\sigma_3' - \sigma_1')^2]} \quad \text{----(1-15)}$$

Von Mises theory presents more accurate results, therefore, will be used to calculate the equivalent strain, and the stress and strain range being cycled to determine if shakedown is achieved.

1.2.3 Concept of Elastic-Perfectly Plastic Material

In a fatigue test, the elastic-plastic material behavior during the initial load-up phase as well as the load-unload cyclic phase is examined. In the plastic region, this is difficult to analyze because engineering metals can strain-harden or strain-soften when deformed at a temperature below their recrystallisation temperature. In such a case, subsequent yield surfaces are applicable after different histories of plastic deformation[9]. Thus, it is convenient to consider the yielding of an elastic-perfectly-plastic metal according to the von Mises and the Tresca yield criteria corresponding to a biaxial stress state or plane stress state. For an elastic-perfectly-plastic material, the yield surface does not change with plastic flow; when a material is cycled through a strain range larger than its yield strain, it has the idealized stress-strain relationship shown in Figure 1.6.

ABAQUS has the capability to analyze the material behavior in the plastic region by using the above assumption. To use an elastic-perfectly plastic algorithm and to define a material which has non-linear characteristics, a parameter, NLGEOM, is added to the STEP card into the ABAQUS input file [12]. Therefore, the results from the fatigue analysis in this thesis will be obtained using the NLGEOM parameter.

The KPL module of the KSHEL computer code developed by Updike and Kalnins (1991) also employs the same algorithm [11]. This module employs shell

elements that can admit arbitrary elastic-plastic material behavior and also account for arbitrarily large deflections, rotations, and plastic strains. Some results obtained from running the KSHEL code will be shown in the later chapters.

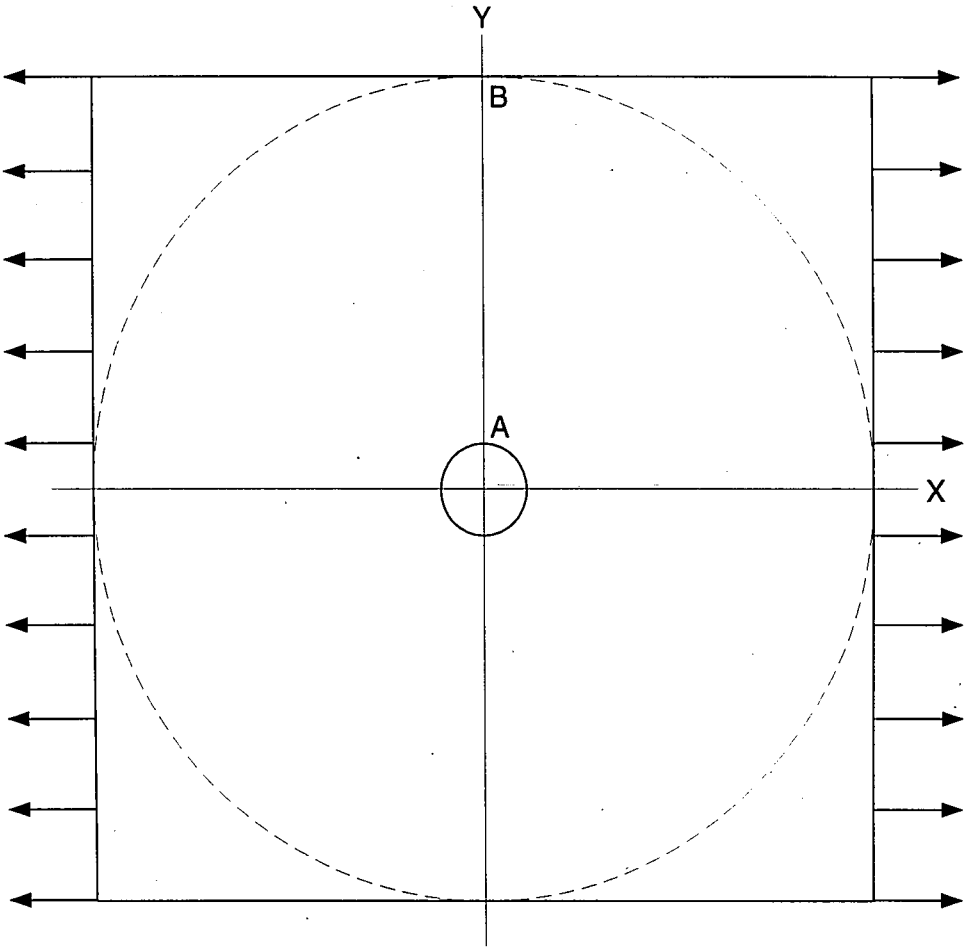

Figure 1.1 Square Plate with Single Circular Hole

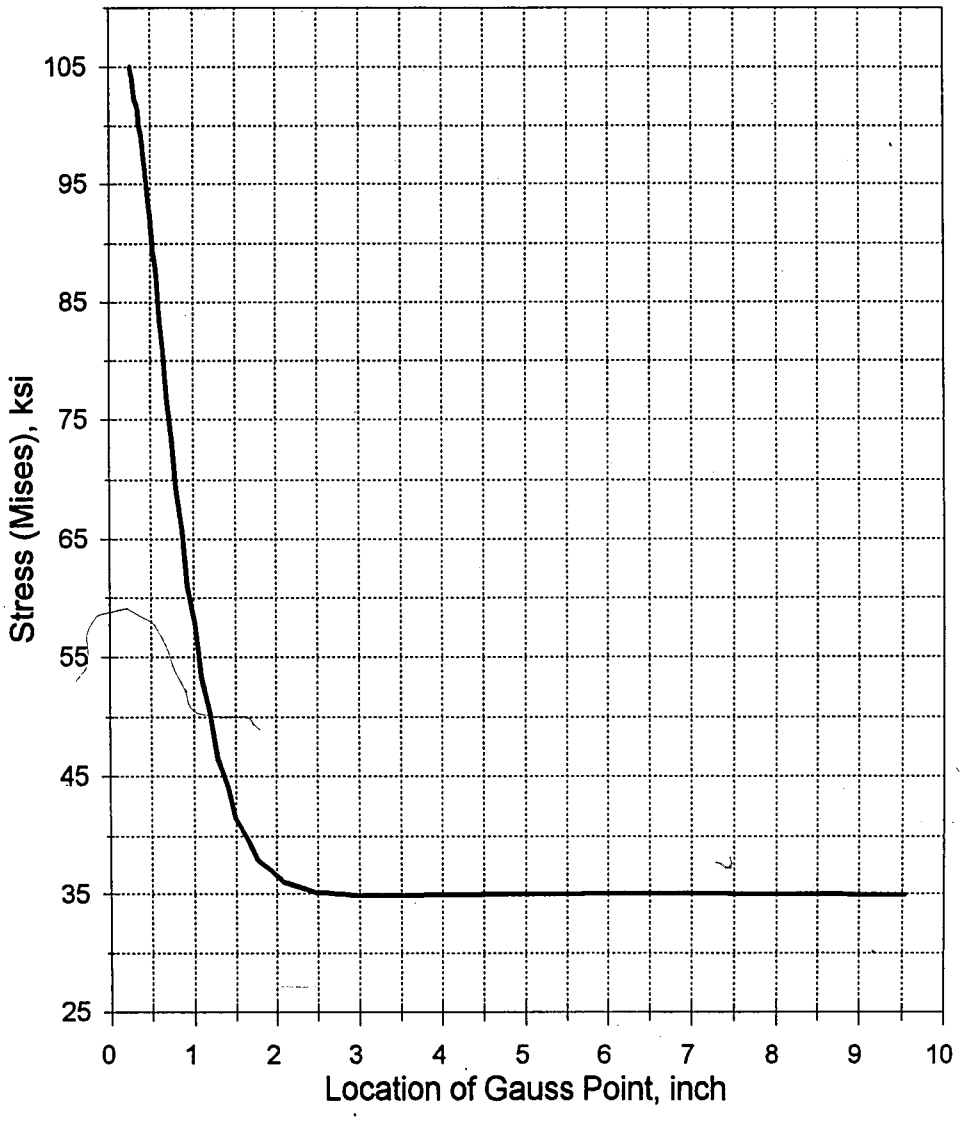

Figure 1.2 Stress Distribution along the Edge perpendicular to the Direction of Traction

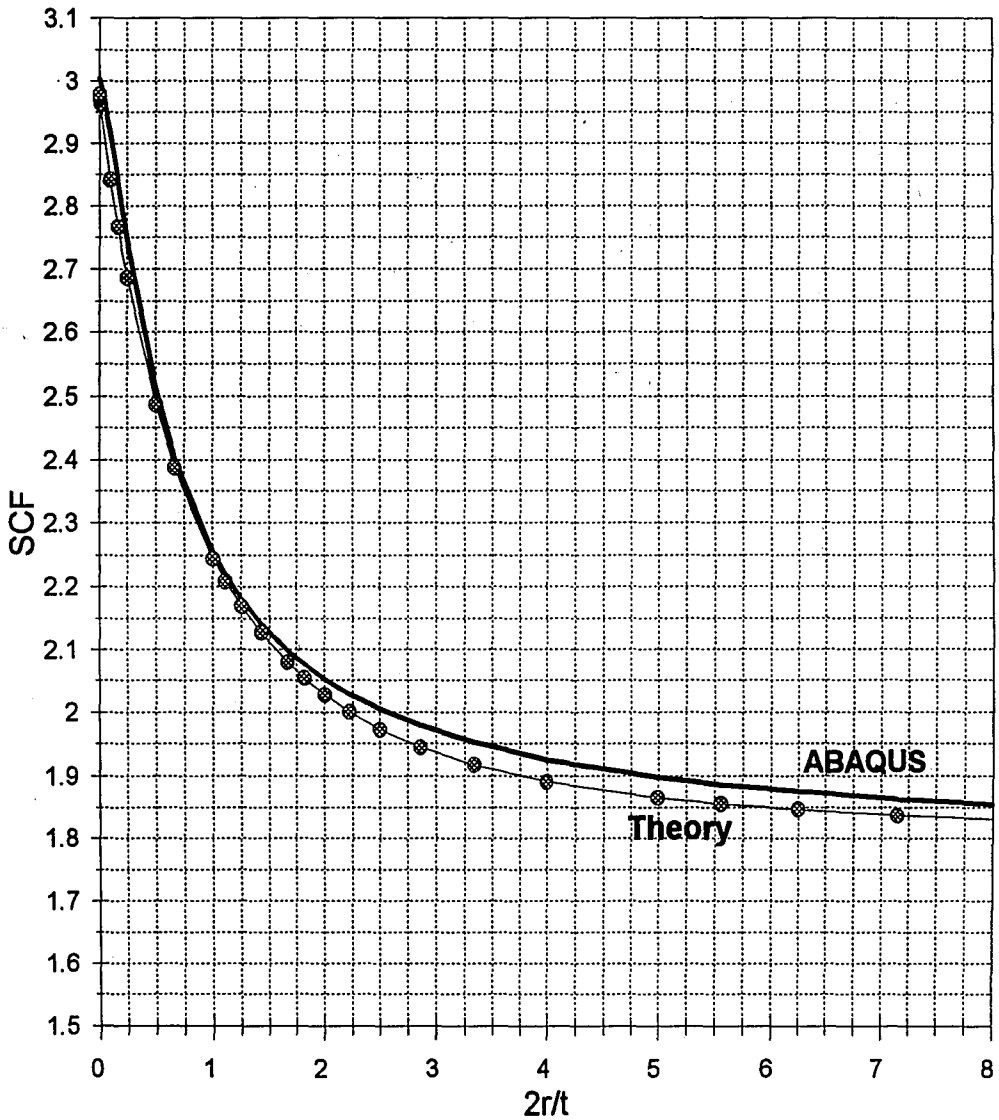

Figuare 1.3 Stress Concentration Factor of the Square Plate with a Hole under Moment

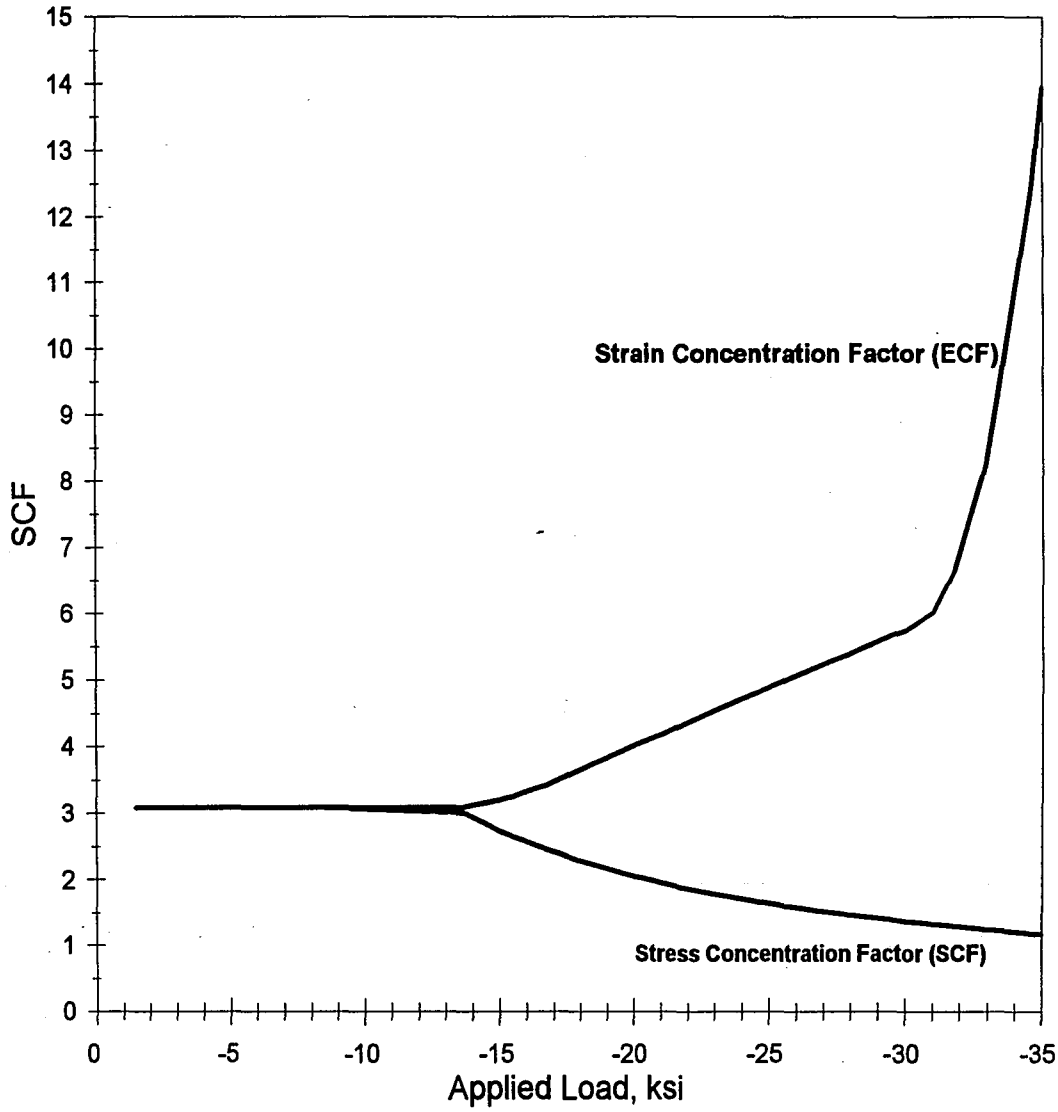

Figure 1.6 Stress and Strain Concentration Factors in Plastic Region When Loading

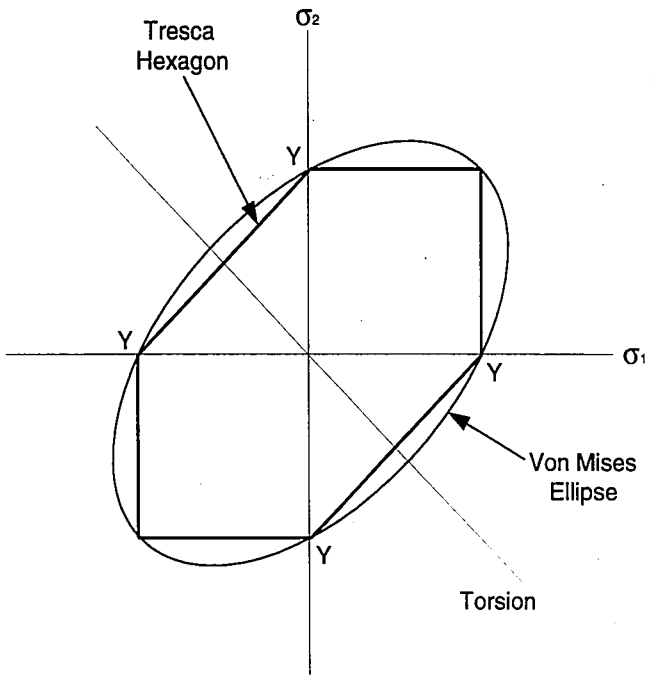

Figure 1.5 Yield Loci for Biaxial Stress according to the von Mises and Tresca Yield Criteria

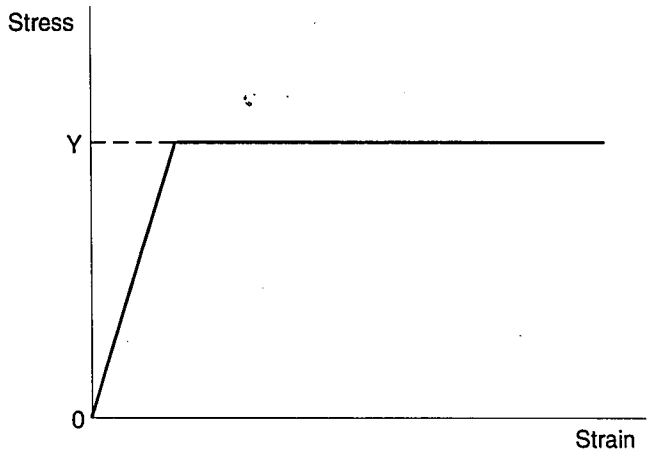

Figure 1.6 Idealized Stress-Strain Relationship for Elastic-Perfect Plasticity

Table 1.1 Elastic SCF in square plate with hole subjected to out-of-plane bending (Radius and Thicknesses in inches, Stresses in psi)

r	t	2r/t	Mises (max)	Far (Mises)	SCF	
					ABAQUS	Theory
0.5	0.05	20.000	1162.0	640.8	1.813	1.804
0.5	0.1	10.000	295.2	160.4	1.840	1.822
0.5	0.12	8.333	206.3	111.4	1.852	1.830
0.5	0.14	7.143	152.5	81.83	1.864	1.838
0.5	0.16	6.250	117.5	62.65	1.875	1.847
0.5	0.18	5.556	93.37	49.49	1.887	1.856
0.5	0.2	5.000	76.08	40.09	1.898	1.865
0.5	0.25	4.000	49.39	25.65	1.926	1.891
0.5	0.3	3.333	34.77	17.81	1.952	1.917
0.5	0.35	2.857	25.89	13.08	1.979	1.945
0.5	0.4	2.500	20.07	10.01	2.005	1.973
0.5	0.45	2.222	16.05	7.912	2.029	2.000
0.5	0.5	2.000	13.16	6.408	2.054	2.028
0.5	0.55	1.818	11.00	5.296	2.077	2.054
0.5	0.6	1.667	9.340	4.450	2.099	2.080
0.5	0.7	1.429	7.003	3.269	2.142	2.127
0.5	0.8	1.250	5.463	2.503	2.183	2.170
0.5	0.9	1.111	4.392	1.978	2.220	2.209
0.5	1	1.000	3.615	1.602	2.257	2.245
0.5	1.5	0.667	1.713	0.7123	2.405	2.387
0.5	2	0.500	1.008	0.4007	2.516	2.488
0.5	4	0.250	0.2755	0.1002	2.750	2.687
0.5	6	0.167	0.1267	4.4509E-02	2.847	2.768
0.5	10	0.100	4.6865E-02	1.6027E-02	2.924	2.842
0.5	100	0.010	4.8115E-04	1.6019E-04	3.004	2.965
0.5	200	0.005	1.2032E-04	4.0047E-05	3.004	2.973
0.5	500	0.002	1.9254E-05	6.4075E-06	3.005	2.978
0.5	1000	0.001	4.8135E-06	1.6019E-06	3.005	2.979

Chapter 2

ANALYSIS OF A SQUARE PLATE WITH A HOLE

2.1 OVERVIEW

Chapter 1 states that elastic analysis of a square plate with a hole were previously performed and results were obtained which indicates a need for further studies. Also, results obtained from employing ABAQUS closely matched those results obtained from theory.

Using the same geometry as the previous chapter, plastic analysis is performed to estimate the strain range and the plastic behavior of a material under cyclic loading. Plastic analysis is performed on two types of loading; in-plane forces and out-of-plane bending moments are employed since a knuckle in a torispherical is subjected to traction and moments. In addition, the concept of shakedown and the characteristics of elements in ABAQUS for a plastic analysis are examined.

2.1.1 Geometry

The geometry shown in Figure 1.1 is the full shape of a square plate with a hole at the center. The model will analyze a quarter of the size of the actual plate. Uniaxial traction is applied to one edge, away from the hole, while the opposite edge, adjacent to the hole is subjected to symmetry constraints. This geometry has three length dimensions: edge length of the quarter-plate b, hole radius a, and plate thickness t. For

the present analysis, the square plate has dimensions b = 10 in., a = 0.5 in., and t = 0.125 in.

The finite element model for the current analysis is shown in Figure 2.1 (a), with the critical element numbers indicated. To acquire accurate results near the hole, a BIAS parameter [12] given by ABAQUS is employed and 20 elements are generated around the hole. The boundary and load conditions are shown in Figure 2.1 (b).

2.1.2 Elements in ABAQUS

ABAQUS provides shell elements for the purpose of various analyses. For a stress/displacement analysis in a torispherical head, S8R and S8R5 with 8 nodes for definition, are employed.

Element type S8R with six degrees of freedom, u_x, u_y, u_z, ϕ_x, ϕ_y, and $\phi_{z,,}$ per node, is normally employed for thick shell applications with respect to the Reissner theory of plates and can be used for modeling cases at which transverse shear flexibility is important. Therefore, the transverse shear resultant forces, Q, are not zero [15,16]:

$$\gamma_{zx} = w_{,x} + \beta_x \qquad \gamma_{yz} = \beta_y + w_{,y} \quad \text{----------(2-1)}$$

where γ_{zx} γ_{yz} = the transverse shear strains

β_x β_y = rotation angles of the normal of the reference plane

$w_{,x}$ $w_{,y}$ = derivatives of deflection with respect to x and y

$$Q_x = GA\gamma_{zx} \qquad Q_y = GA\gamma_{yz} \quad \text{----------(2-2)}$$

where Q_x Q_y = the transverse shear resultant forces

A = the section area

On the other hand, element type S8R5 employs five degrees of freedom, u_x, u_y, u_z, and two in-surface rotations, per node, which is intended for thin shell application with respect to the classical plate theory. Therefore, when transverse shear stress is not important, this element can be used.

Analysis results of simple models including element S8R and S8R5 are compared in Table 2.1; the maximum stress for both S8R and S8R5 is found at the same location, element 20 (EL20), and the stress concentration factors for each are similar in magnitude, suggesting that either element can be used for an elastic analysis without any problems if the external force is tension or moment. However, in plastic analysis, if bending from an external force is found as a secondary effect, employing the S8R5 element is not appropriate because the S8R5 element uses 5 degrees of freedom at all nodes and does not calculate for the effects of transverse shearing. When this element is employed for plastic analysis while a rotation of the normal of element from transverse shearing is produced in the plastic region, after many iterations, ABAQUS issues error messages pertaining to equilibrium convergence. The S8R5 element can be switched to an element which uses 6 degrees of freedom at all nodes, like S8R element, if the following conditions are met [12]:

When any nodes being included in the S8R5 element

- has a *BOUNDARY condition on a rotational degree of freedom, or
- is involved in an MPC that employs rotational degrees of freedom, or

- is attached to a beam or a shell element that uses six degrees of freedom at all nodes,

or

- is a point where different elements have different surface normals, or
- is loaded with moments,

that it seems that this element can not fully support material behaviors in the plastic region. Therefore, for the plastic analysis which may retain transverse shearing, the S8R element is a better choice than the S8R5 and all models analyzed for the present thesis, are constructed by using the S8R element.

2.1.3 Shakedown

In low cycle fatigue, shakedown is one of the important factors. Shakedown occurs when cyclic loads are applied to the material, after first yielding, there exists no further plastic straining for a number of cycles. When in-plane traction, far from a local discontinuity, reaches limiting values, yielding begins around the local discontinuity, assuming elastic-perfectly plastic material behavior. If the edge traction increases further, plastic strains are produced at the local discontinuity. Then, if unloading occurs and the far-field traction is reduced back to zero without any reverse yielding and if no additional plastic strain is produced, shakedown is achieved. Kalnins and Updike [17] examine the ways in which shakedown is achieved by calculating the stress intensity range being cycled. They introduce yield surface of von Mises theory to explain whether or not shakedown is achieved.

2.2 TRACTION BY IN-PLANE FORCES

The types of applied loads should be defined as concentrated forces in order to solve problems by using the ABAQUS FE code, since elements used in a square plate are shell elements, S8R, having eight nodes for definition. Concentrated forces applied to the boundary nodes are calculated by employing a finite element method (FEM) [17] shown in Figure 2.1 (b) with vector magnitudes.

2.2.1 Elastic Analysis

The elastic stress concentration factor (SCF) and the location of the highly stressed element are obtained from an elastic analysis; the results indicate that if a far-field stress, S11 = 26.67, then the most highly stressed element lies at the rim of the hole, element 20 (EL20 in Figure 2.1 (a)), and its value, S11 = 80.22, which confirms that SCF = 3. Also, the maximum stress of element 1 (EL 1 in Figure 2.1 (a)) is S22 = – 26.89 which validates equation (1-4), which predicts that S22 is equal to the negative far-field stress. The deformed shapes around the hole are elliptic and are shown in Figure 2.2.

2.2.2 Plastic Analysis

2.2.2.1 Traction up to Shakedown Limit

When the in-plane traction in the far-field reaches a third of the yield strength, Y/3, yielding begins in element 20 (EL20), assuming elastic-perfectly plastic material behavior. Increase in edge traction results in plastic strains at the hole. However, if a

comparison of the stress and the total strain in EL20 at the hole is desired, the plastic straining in EL20 can only be determined from elastic-plastic analysis. The stress versus strain relation from elastic-plastic analysis, assuming that the material is initially stress-free, is shown in Figure 2.3.

Figure 2.3 indicates that the external load is applied initially at Point 0 until the first yield, which occurs at Point A and continues to yield to Point C. The first half cycle is defined as 0A under elastic deformation and AC under plastic deformation. When the far-field stress, σ_0 = 2Y/3, the total strain in EL20 is at Point C with value, E11 = 0.00458. If the far-field stress is reduced back to zero, unloading at EL20 follows the elastic curve, down to Point D, with no reverse yielding. If further cycling occurs, the stress follows the path between Point C and Point D, hysteretically. Since no reverse yielding occurs, the straight path is completely elastic, which means shakedown is achieved. Thus, σ_0 = 2Y/3 is the highest traction at which shakedown occurs when SCF = 3.

The cycled equivalent strain range is calculated as E_{Range} = 0.00274. By using E_{Range}, the alternating stress being cycled after obtaining shakedown can be calculated:

$$\sigma_{alt} = \frac{1}{2} E_{Range} E \quad \text{---------- (2-3)}$$

where σ_{alt} = alternating stress being cycled

E_{Range} = equivalent strain range being cycled

E = Young's modulus

Point B in Figure 2.3 represents a fictitious elastic stress while the distance between Point G and Point B is a fictitious elastic strain. Furthermore, since the line 0B and CD are of equal length and oriented at the same angle, the fictitious elastic equivalent strain, $E_{eq} = 0.00274$; in this case, the elastic analysis gives the same result for the total strain estimate as the plastic analysis.

2.2.2.2 Traction past Shakedown Limit

Even though the far-field edge traction greater than $\sigma_0 = 2Y/3$ may not be permitted in some design codes, it is of interest to inquire how Figure 2.3 would change if this limit was exceeded. Assume that the far-field stress σ_0 goes up to 5Y/6 then returns back to zero, repetitively reloading and unloading. Figure 2.4 indicates that when the far-field stress is increased, the first half-cycle follows the path 0AC. The total strain in EL20 is at Point C and has the value of E11 = 0.00958. Compared to Figure 2.3, the total strain in EL20 is 2.09 times larger at Point C while the far-field stress is 1.25 times greater. During unloading, the second half-cycle goes from Point C to D elastically but reaches the compressive yield stress from Point D to E, without any increase in compressive stress, but with reverse yielding. Further cycling is indicated by the parallelogram CDEF. Clearly, plastic strain is produced for each cycle. The cycled strain range of E11 equals $E11_{Range} = 0.00369$, which is indicated by the difference in strain at Point C and E. Based on von Mises theory, the equivalent strain range is calculated as $E_{Range} = 0.00374$.

In Figure 2.4, the strain range by elastic analysis is 0.00334 with respect to the E11 component and 0.00352 from von Mises theory. This range can be calculated from the theory of elasticity by $3 \times (5 / 6) \times (Y / E) = 0.00333$ where Young's Modulus E = 30,000 and yield strength Y = 40.0. The calculated values based on the theory of elasticity shows that the magnitude of the range is less than 0.00369 or 0.00374 which were predicted from the elastic-plastic analysis. This result indicates that while the elastic stress concentration factor (SCF) is three, the cyclic strain range concentration factor (ECF) is now 3.32 on the E11 component and 3.37 using von Mises theory. It also shows that, for this case, fatigue analysis based on elastic analysis is not conservative. The difference between elastic and plastic analysis is shown in Figure 2.4 where Point B represents a fictitious elastic stress. Therefore, elastic-plastic analysis is a more effective way to estimate the lifetime of a material under cyclic loading.

2.2.3 Strain Range (E_{Range})

The cyclic strain range is determined from the strain components of two points, C and E in Figure 2.4, after loading and unloading. To calculate the values of the three strain components, the loading and unloading half-cycles are needed; with one more calculation step, the total equivalent strain range can also be determined.

There is one way to calculate the total strain range with just one half-cycle: Figure 2.4 shows that unloading occurs at EL20, as the second half-cycle goes from Point C to D elastically with a magnitude of 2Y. If the yield strength is defined as 2Y in

the ABAQUS input file, the second half-cycle stress-strain history curve during unloading will be obtained as the first half-cycle curve.

The result is plotted in Figure 2.5. It shows that during the first half-cycle the stress at EL20 increases elastically up to 2Y at Point A, followed by plastic straining continuing to Point B. The total strain is E11 = 0.00372 and the equivalent total strain is E_{eq} = 0.00378. The magnitudes of the strain range are slightly greater than those shown in Figure 2.4. It is assumed that these minor differences may be attributed to the difference in the time steps being used in the ABAQUS FE code; due to the time steps, the maximum far-field stress found in Figure 2.4 equals 33.29 while it is 33.30 in Figure 2.5.

2.2.4 Calculated Data

The ABAQUS FE code calculates stress and strain components in global XYZ coordinates. For a shell element, the stress components are S11, S22, S12, and the strain components are E11, E22, E12. Von Mises stress intensity, in terms of all stress components, is expressed by

$$MISES = \sqrt{\frac{1}{2}\left[\left(\sigma_x - \sigma_y\right)^2 + \left(\sigma_y - \sigma_z\right)^2 + \left(\sigma_z - \sigma_x\right)^2\right] + 3\left(\tau_{xy}^{\ 2} + \tau_{yz}^{\ 2} + \tau_{zx}^{\ 2}\right)} \quad \text{---- (2-4)}$$

According to the classical shell theory, the transverse normal stress, σ_z, is negligible when compared to the in-plane stresses, σ_x, σ_y, and $\tau_{yz} = \tau_{zx} = 0$. Then, von Mises stress intensity is simplified to

$$MISES = \sqrt{S11^2 + S22^2 - S11S22 + 3S12^2} \quad \text{---------- (2-5)}$$

with respect to the stress components employed in ABAQUS.

When the three principal strains are ε_1 , ε_2 ,and ε_3 , the equivalent strain is defined by [10]

$$E_{eq} = \frac{\sqrt{2}}{3}\sqrt{(\varepsilon_1 - \varepsilon_2)^2 + (\varepsilon_2 - \varepsilon_3)^2 + (\varepsilon_3 - \varepsilon_1)^2} \quad \text{----------(2-6)}$$

and in terms of non-principal strains,

$$E_{eq} = \frac{1}{3}\sqrt{(\varepsilon_x - \varepsilon_y)^2 + (\varepsilon_y - \varepsilon_z)^2 + (\varepsilon_z - \varepsilon_x)^2 + 6(\varepsilon_{xy}^2 + \varepsilon_{yz}^2 + \varepsilon_{zx}^2)} \quad \text{-----(2-7)}$$

In plasticity, it is assumed that plastic deformation is incompressible, which is expressed as

$$d\varepsilon_1^p + d\varepsilon_2^p + d\varepsilon_3^p = 0 \quad \text{----------(2-8)}$$

where $d\varepsilon_1$, $d\varepsilon_2$, and $d\varepsilon_3$ are principal strain increments and the superscript, p, denotes plastic strain. Thus, the equivalent plastic strain is defined as

$$E_{eq}^{\ p} = \int \sqrt{2/9\left[(d\varepsilon_1^p - d\varepsilon_2^p)^2 + (d\varepsilon_2^p - d\varepsilon_3^p)^2 + (d\varepsilon_3^p - d\varepsilon_1^p)^2\right]} \quad \text{--------(2-9)}$$

From equation (2-6) and (2-8), the total true equivalent strain is given by

$$E_{eq} = \frac{2}{\sqrt{3}}\sqrt{\varepsilon_1^{\ 2} + \varepsilon_2^{\ 2} + \varepsilon_1\varepsilon_2} \quad \text{----------(2-10)}$$

or in terms of strain components employed in ABAQUS

$$E_{eq} = \frac{2}{\sqrt{3}}\sqrt{E11^2 + E22^2 + E11E22 + (E12/2)^2} \quad \text{----------(2-11)}$$

The cyclic equivalent strain range is calculated from the strain components at the beginning and the end of the second half-cycle, denoted C and E in Figure 2.4. The range is given by

$$E_{Range} = \frac{2}{\sqrt{3}}\sqrt{(E11_E - E11_C)^2 + (E22_E - E22_C)^2 + (E11_E - E11_C)(E22_E - E22_C) + (E12_E - E12_c)^2/4} \quad \text{----------(2-12)}$$

where the subscripts, E and C, corresponds to Points E and C in Figure 2.4.

2.2.5 Stress/Strain Concentration Factors in the Second Half-Cycle (SCF, ECF)

In the previous chapter, the relationship between the stress/strain concentration factor, K_t and K_ε , in the plastic region, was considered for the first half-cycle. After loading, if unloading follows as a second half-cycle, the curves in Figure 1.4 may be different. The results from ABAQUS for the second half-cycle is shown in Figure 2.6. For the first half-cycle, K_t = 1.17 and K_ε = 13.94. When the far-field stress is reduced back to zero, the stress concentration factor K_t decreases until the far-field stress equals −22.12, then begins to exponentially increase. However, the strain concentration factor K_ε increases continuously for the first half-cycle; when the far-field stress and strain have zero magnitudes at the end of the second half-cycle, the stress and strain at highly stressed element still have some magnitudes. Thus, the calculated SCF and ECF increases exponentially to infinity, which indicates that in plastic region, the calculated concentration factors, K_t and K_ε, are meaningless. Therefore, the stress and the strain

range should be considered as the important factors instead of the two concentration factors.

2.3 TRACTION BY MOMENTS

2.3.1 Elastic Analysis

When moments are applied to the edge where x = constant, the solution from theory of elasticity predicts an elastic stress concentration factor (SCF) dependent on the hole diameter and the plate thickness ratio, 2r/t, as shown in Figure 1.3. All related equations are stated in the previous chapter. According to equation (1-6), for a Poisson's ratio of 0.3, the SCF at element 20 (EL20) is 1.79 and 0.21at element 1 (EL1).

A FE solution by ABAQUS indicates that, if far-field stress, S11 = 40.0, then for EL20, the highly stressed element, the stress, S11 = 74.41, giving a SCF of 1.86, while the maximum stress in EL1 is S22 = 6.039, giving a SCF = 0.15. The results from ABAQUS are slightly high and low in comparison to the results from the theory of elasticity. It is deduced that these differences were produced because all stress components from ABAQUS are not calculated at node points but at Gauss points.

2.3.2 Plastic Analysis

When out-of-plane bending moments with magnitudes, $M_0 = (t^2\ Y) / 6$, are applied to the edge where x = constant, where yield strength, Y = 40.0 and plate thickness t = 0.125, ABAQUS produces results shown in Figure 2.7 and Figure 2.8.

Due to the out-of-plane bending, the outside surface of the plate is in compression while the inside surface is under tension.

At the end of the first half-cycle when the far-field stress, S11 = 40.01, at the inside surface, the total strain in the most strained element, EL20, is at Point C in Figure 2.7 and has the value of E11 = 0.00322. The second cycle starts at Point C and follows the elastic curve until Point D, with no reverse yielding. Further cycling follows the path between Point C and D, hysteretically, but there is no reverse yielding and the path is all elastic. This indicates that, when $M_0 = (t^2 Y) / 6$, shakedown is achieved. The value of $M_0 = (t^2 Y) / 6$ can be calculated by using the plastic moment M_p. The plastic moment is expressed as

$$M_p = \frac{1}{4} t^2 Y \quad \text{----------(2-13)}$$

If the safety factor, 2/3, is applied to the plastic moment, M_0 can be obtained directly. Thus, $M_0 = (t^2 Y) / 6$ is the highest moment at which shakedown occurs. The cycled strain range is $E11_{Range} = 0.00273$ and the cycled equivalent strain range is $E_{Range} = 0.00280$.

From the elastic solution, the fictitious elastic strain at Point B in Figure 2.7 has the value of E11 = 0.00248 and $E_{eq} = 0.00255$. It is assumed that these differences between plastic and elastic analyses are derived from material behaviors with respect to the NLGEOM [12] parameter in the ABAQUS code. Once again, it is proven that plastic analysis is more effective in achieving accurate results.

For the out-of-plane bending moment, compression occurs on the outside surface. The result is shown in Figure 2.8. Contrary to the inside surface, the stress-strain history curve is in the negative region of the strain axis. The total compressive strain in EL20 is at Point C in Figure 2.8 and has the value E22 = –0.00284. When the far-field stress returns to zero, the unloading path in EL20 is all elastic to D, with no reverse compressive yielding. In this case, the cycled strain range $E11_{Range}$ = 0.00245, in compression and the cycled equivalent strain range, E_{Range} = 0.00252. These two values are less than that of the inside surface; elastic-plastic analysis indicates different strain magnitudes between the outside and inside surfaces while the elastic analysis indicates same magnitudes but opposite signs (i.e. positive for tension and negative for compression). It is confirmed again that the elastic-plastic analysis is more effective.

In Figure 2.9, the true von Mises stress intensity at the most strained element, EL20, is plotted against the applied moment steps. The two curves indicates the inside and outside surfaces. At the first half-cycle, yielding takes place on both inside and outside surfaces for ten steps then at the second unloading half-cycle, no reverse yielding is found. For further cycling, no further plastic actions are detected in the figure. It is again confirmed that shakedown has been achieved.

2.4 TRACTION BY IN-PLANE FORCES AND MOMENTS

For the geometry of a hole in the knuckle of a torispherical head, the in-plane and bending actions are combined. Without the hole, the knuckle experiences circumferential compression with little bending, meridional stretching and bending inward, which

produces tension on the inside surface and compression on the outside surface. This indicates that the results of the in-plane force and moment solutions for the plate are combined, according to the relative stretching and bending magnitudes.

When the in-plane forces 2Y/3 are applied as shown in Figure 2.1 (b) and the moments $(t^2Y)/6$ are applied along the edge, y = constant, perpendicular to the edge at which forces are being applied, ABAQUS results show that, if the far-field stress S_{MISES} = 58.01 at the outside surface under the compression, then the most compressed element is EL 1 and has the value S_{MISES} = 101.3, giving an SCF = 1.75. The most tensioned element at the inside surface is EL20 and has the value S_{MISES} = 85.85, giving an SCF = 1.48.

When both in-plane forces and moments are applied along the edge, x = constant, the results show that, if the far-field stress, S_{MISES} = 66.54 at the inside surface, then the highly stressed element is EL20 and has a value of S_{MISES} = 154.6, giving an SCF = 2.32. From the above results, it is seen that, if this combined load is applied, the SCF is reduced from 22.7 to 50.7 percent. It is clearly evident that, when the combined load is employed, the elastic SCF of the square plate does not exceed three and shakedown is achieved..

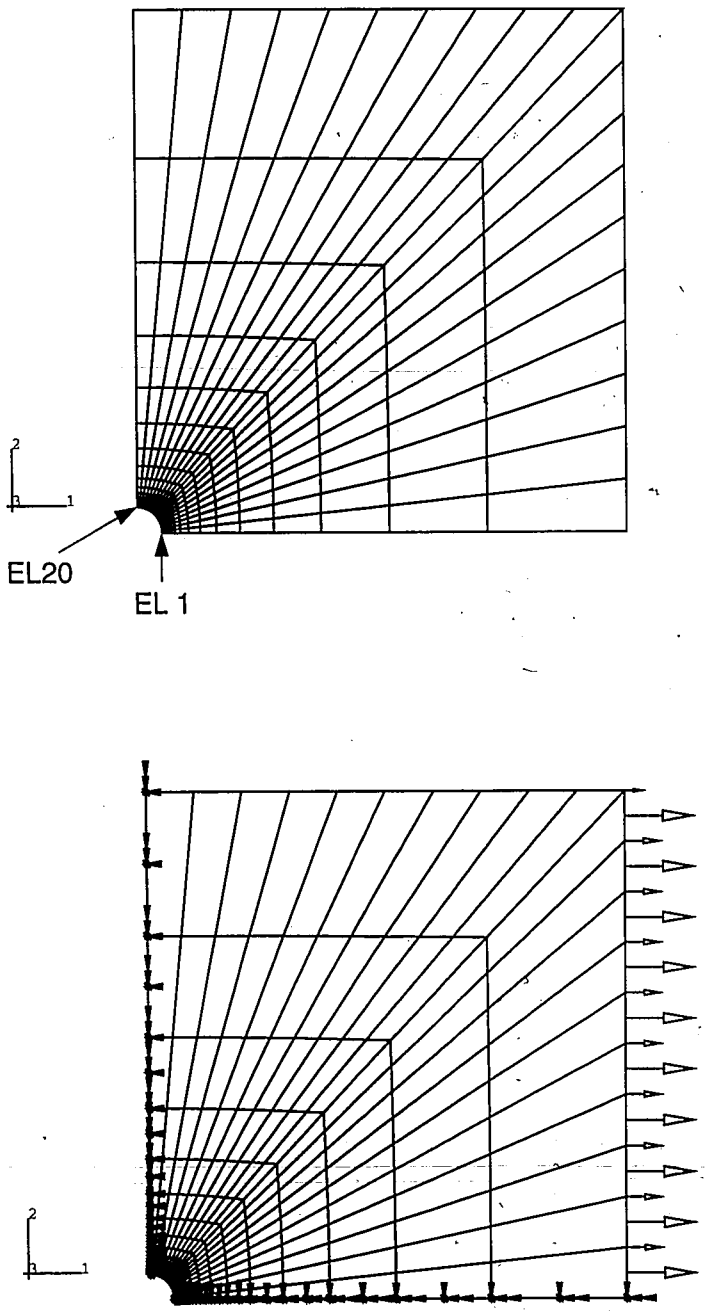

Figure 2.1 Finite Element Mesh for Square Plate with a Hole

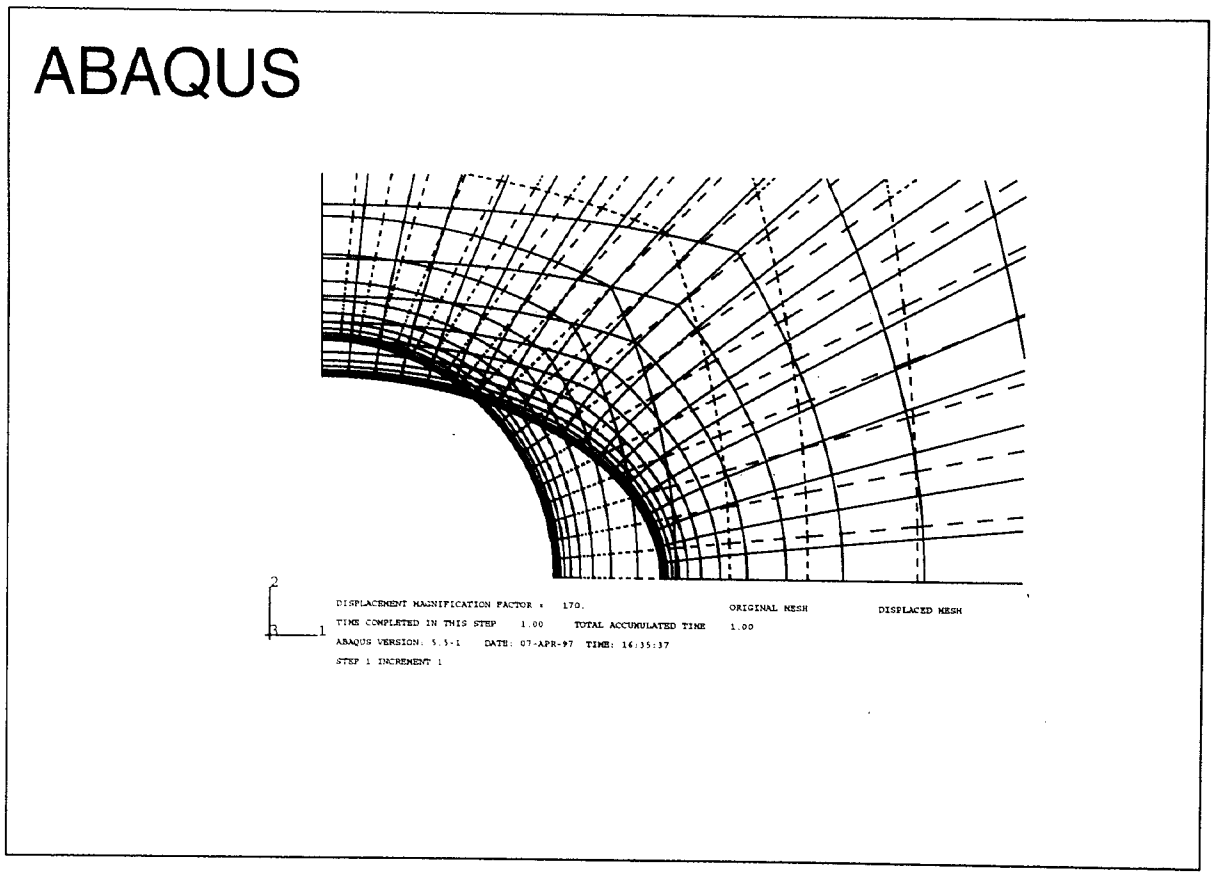

Figure 2.2 Deformed Shape of the Hole under Uniaxial Tension

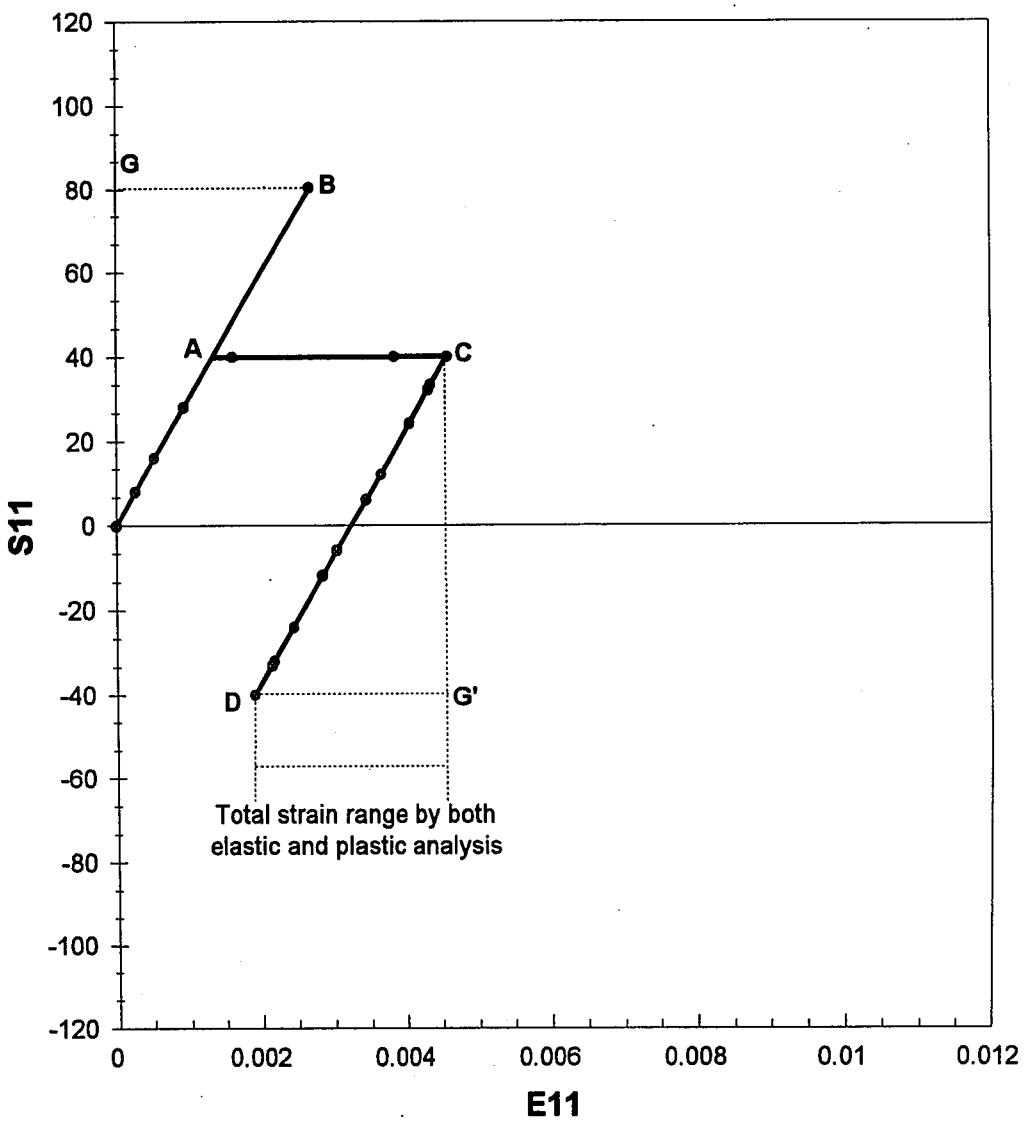

Figure 2.3 Stress-Strain Behavior at Hole for Plate in Cycled Tension When Shakedown Occurs

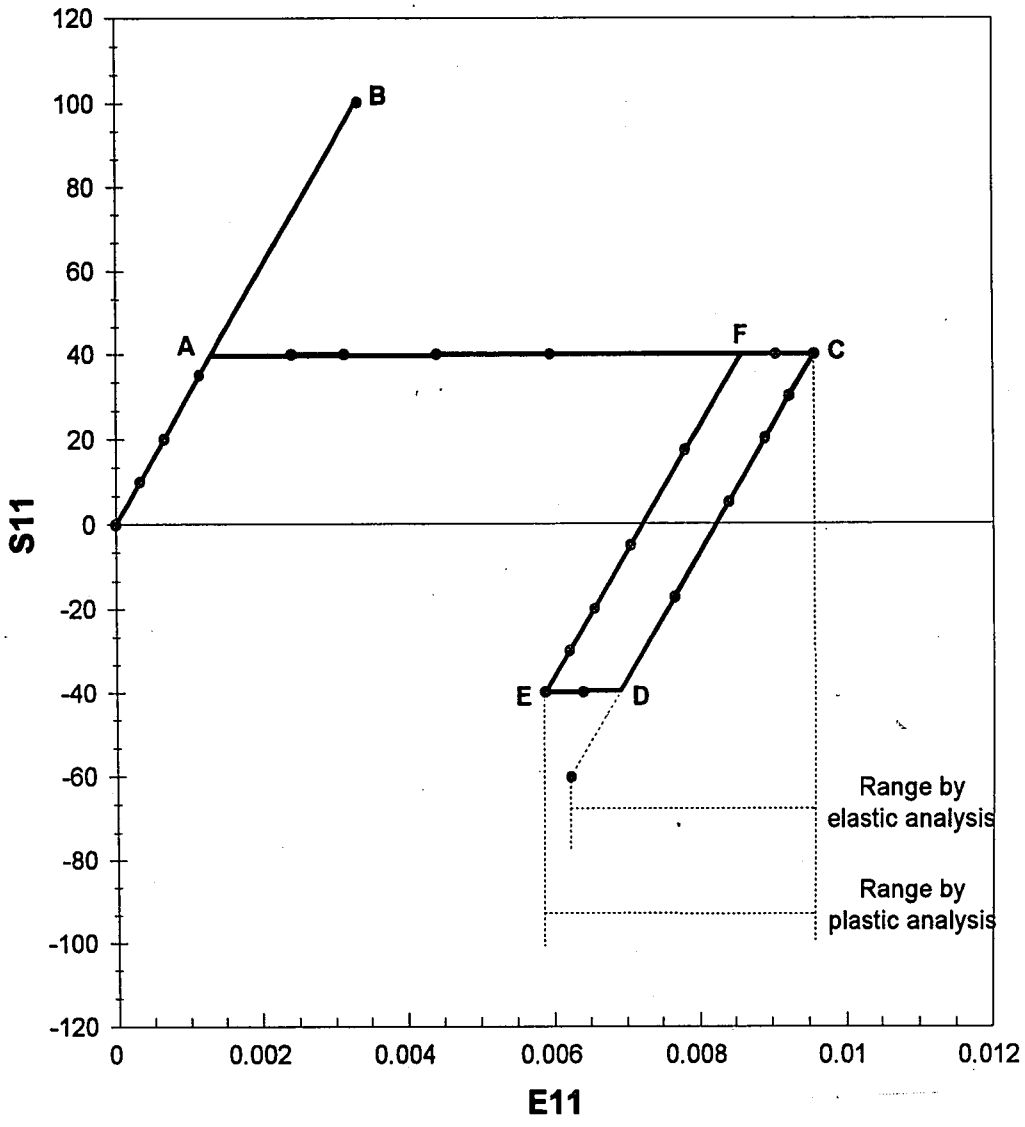

Figure 2.4 Stress-Strain Behavior at Hole for Plate in Cycled Tension When Shakedown Does Not Occur

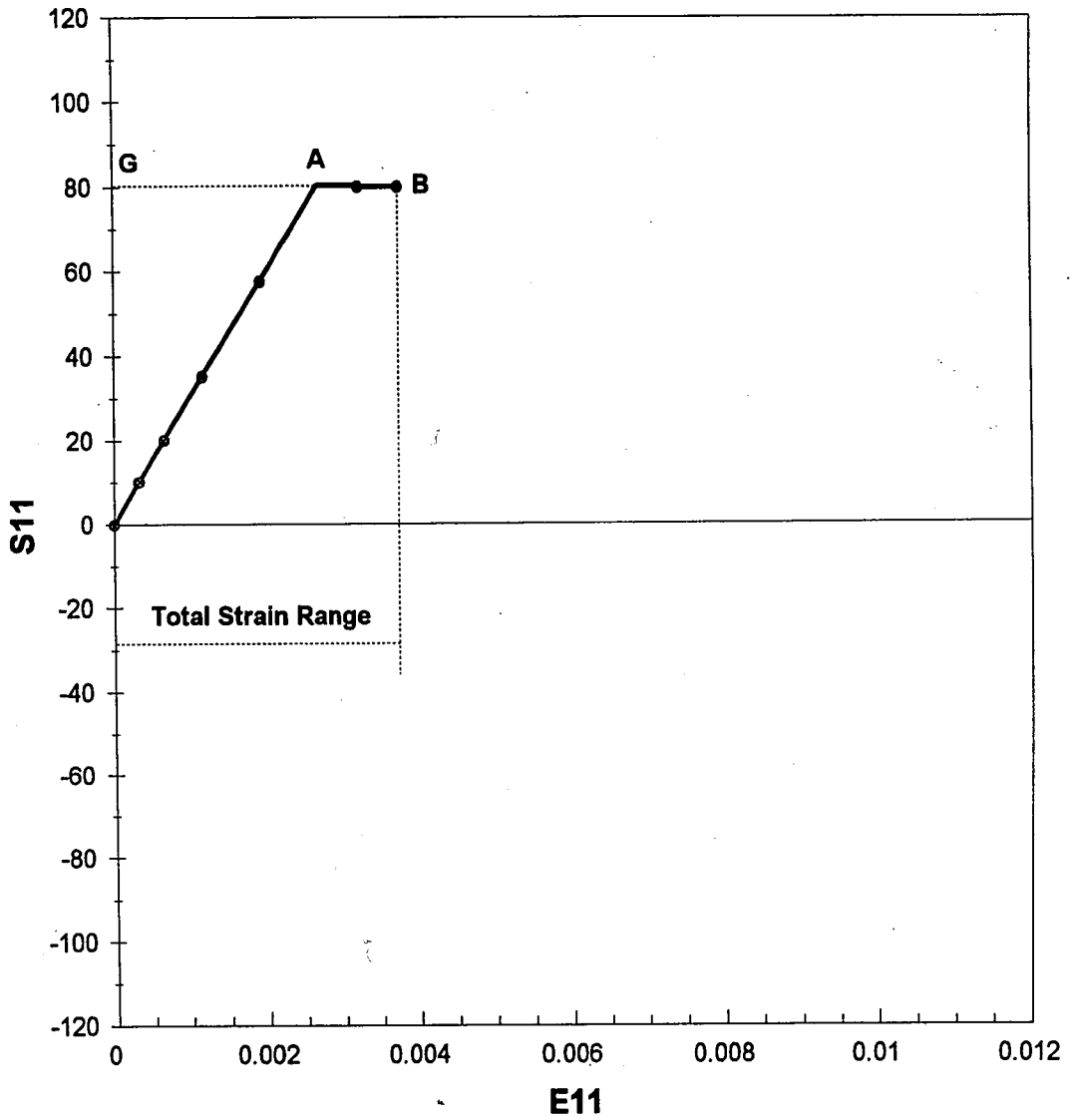

Figure 2.5 Stress-Strain Behavior at Hole for Plate in Tension When Yield Strength is 2Y

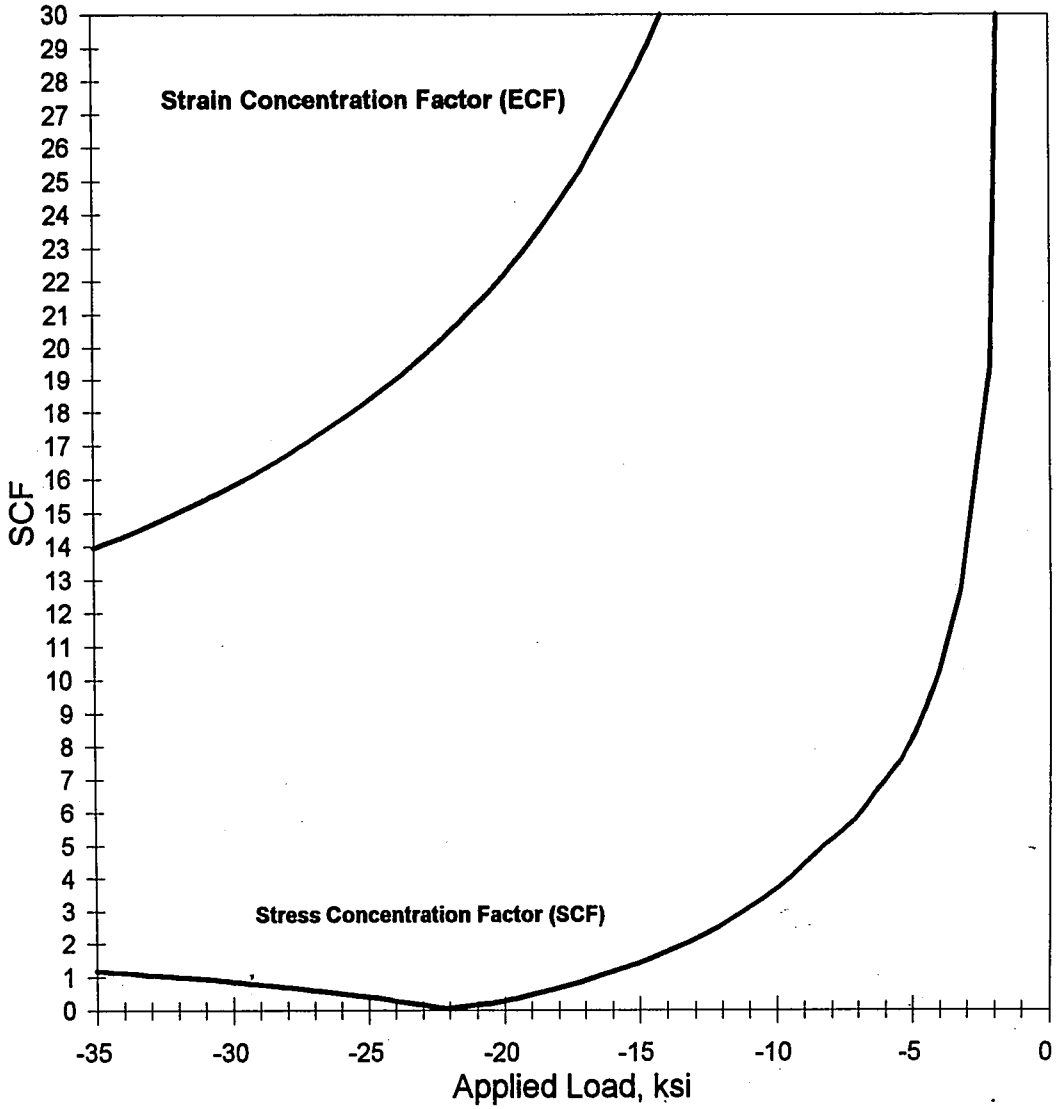

Figure 2.6 Stress and Strain Concentration Factors in Plastic Region When Unloading

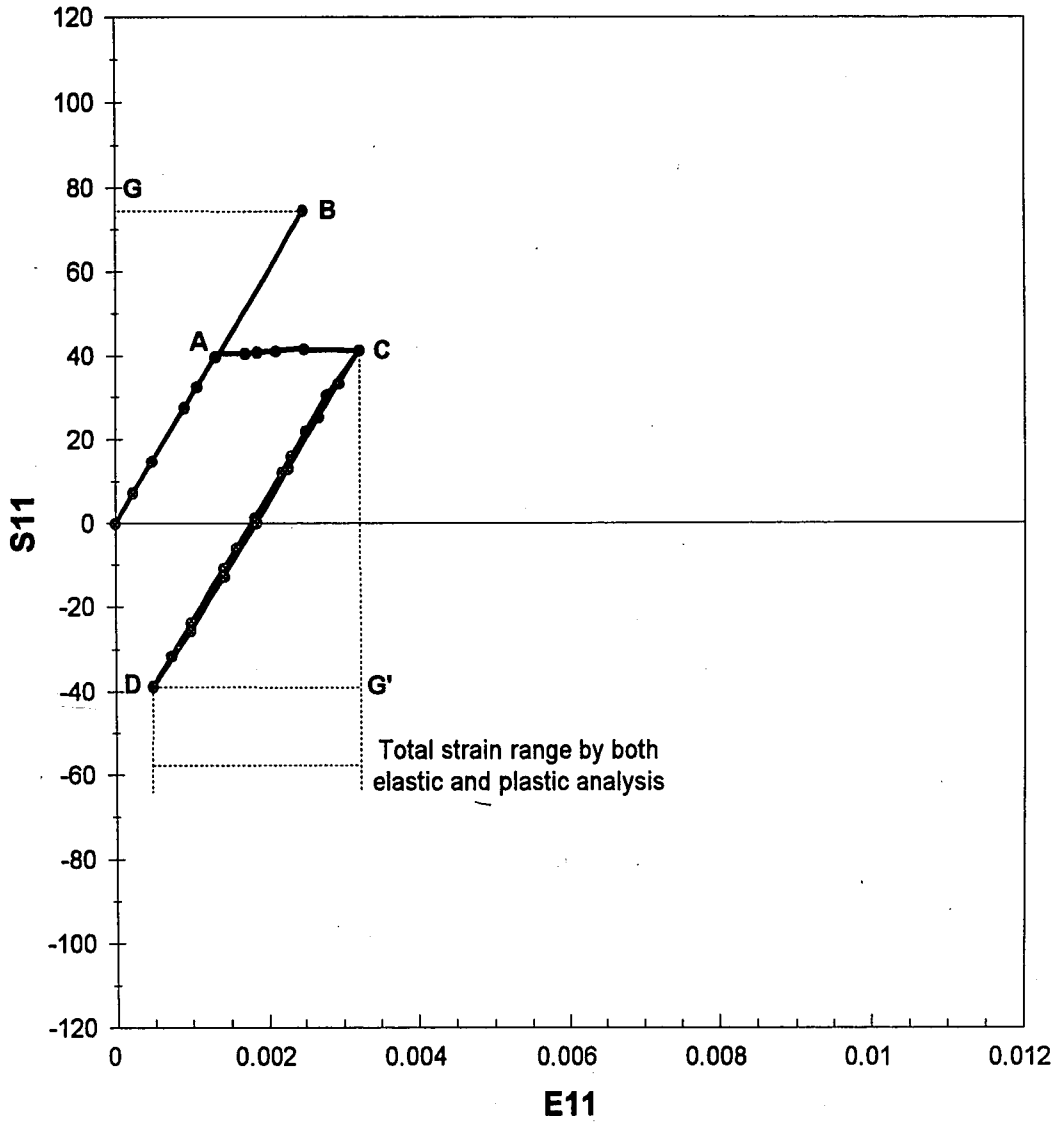

Figure 2.7 Stress-Strain Behavior at Hole for Inside Surface of Plate in Cycled Moment

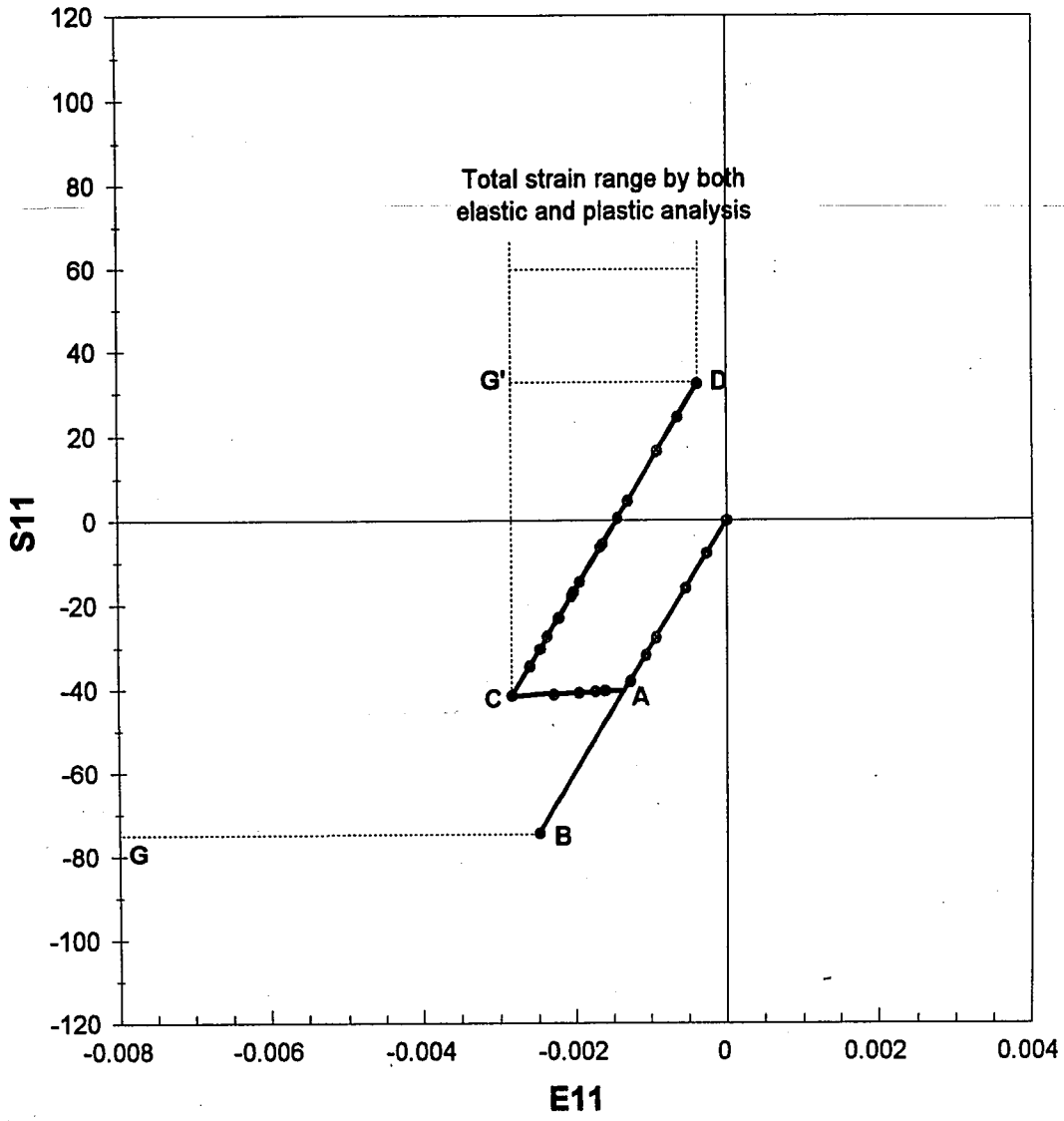

Figure 2.8 Stress-Strain Behavior at Hole for Outside Surface of Plate in Cycled Moment

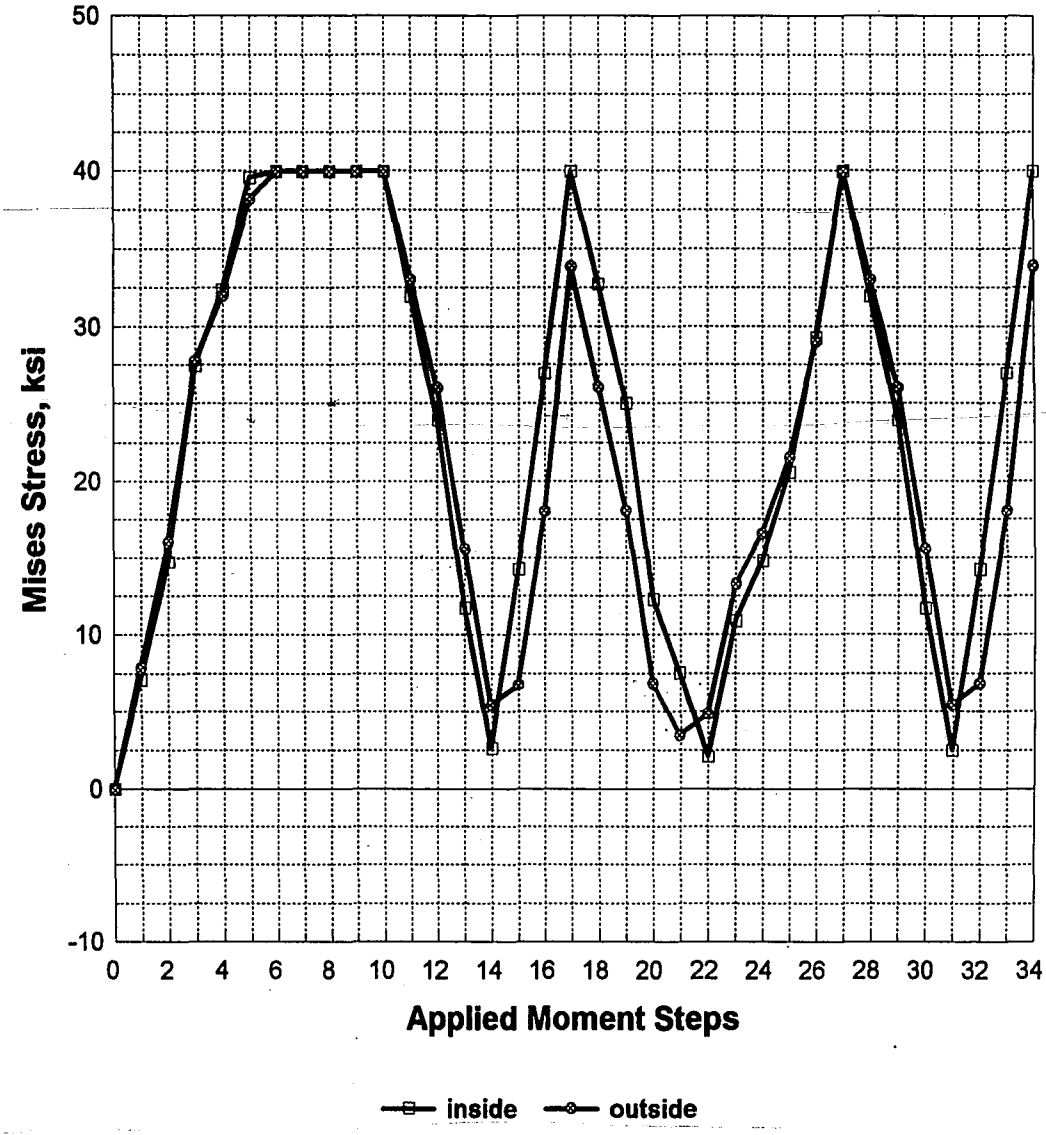

Figure 2.9 Von Mises Stress History at Most Strained Element near the Hole

Table 2.1 Comparing element types, S8R5 versus S8R, with elastic analysis (Stresses in ksi)

TENSION				MOMENT			
Applied Load	GAUSS Point	MAX Stress		Applied Load	GAUSS Point	MAX Stress	
		S8R5 (5 DOF)	S8R (6 DOF)			S8R5 (5 DOF)	S8R (6 DOF)
26.6667	1 1	79.54	79.55	40.0000	1 1	75.37	75.80
	1 5	79.54	79.55		1 5	75.37	75.80
	2 1	78.98	78.97		2 1	75.47	75.33
	2 5	78.98	78.97		2 5	75.47	75.33
	3 1	79.93	79.93		3 1	75.99	76.05
	3 5	79.93	79.93		3 5	75.99	76.05
	4 1	79.35	79.35		4 1	75.36	75.59
	4 5	79.35	79.35		4 5	75.36	75.59
EL #		EL20	EL20			EL20	EL20
SCF		2.997	2.997			1.900	1.901

Chapter 3

ANALYSIS OF A SQUARE PLATE WITH A NOZZLE

3.1 OVERVIEW

In the previous chapters, a square plate with a hole as a local discontinuity has been investigated. Now, a model with an addition of a nozzle to the hole, where the nozzle is welded to the plate, is examined using elastic analysis as shown in Figure 3.1. Welding defects such as porosity, slag inclusions, shrinkage cracks, and surface roughness, can affect the stress concentration of the material and reduce the strength. However, in the present study, it is assumed that the metallurgical structure of the weld metal is identical to the parent metal and assumed that there are no flaws due to welding.

When edge traction produced by in-plane forces is applied to a structure, bending occurs in the vicinity of the nozzle. A section of the nozzle is modeled with axisymmetric elements, as shown in Figure 3.2 and the deformed shape with respect to the edge traction is shown in Figure 3.3. In Figure 3.3, the nozzle part is deformed downward from the vertical axis and bending action is clearly present. For this configuration, the maximum stresses have been found experimentally at two locations [18]: the inside corner, A, and the outside corner, B, of the nozzle (see Figure 3.2). According to John F. Harvey [18], the peak stresses can be minimized at the inside corner, A, by rounding this corner to a radius equal to 25 to 50 percent of the thickness

of the vessel wall. The outside corner, B, can also be altered by rounding with a radius of the same proportion or by applying a taper with a transition radii.

However, E. C. Rodabaugh [19] states that, at A, there is no significant effect on the maximum stress, from changing the square corner to a rounded corner as shown in Figure 3.4. ABAQUS results indicates that for both cases, the maximum stress is the hoop stress, S33, and has the value of 2.077 for the square edge and 1.948 for the rounded edge for an applied load of 1.0 ksi, which indicates a stress reduction is only 6.2 percent. Von Mises stress intensity is 2.055 for the square edge and 1.869 for the rounded edge, resulting in a stress reduction of 9.1 percent. These results suggest that for the inside corner, the square geometry has little effect on the maximum stress. In both cases, hoop stress plays an important role for the crack propagation in the proximity of the hole.

In addition, the ABAQUS results show that stresses at the outside corner, B, are smaller than those at the inside corner, A. At both corners, longitudinal and hoop stresses are tensile and are compared in Figure 3.5. The figure shows that, even though the longitudinal stress of the inside corner at location 20 is smaller than that of the outside corner, the hoop stress of the inside corner is much greater. It can be assumed that a crack will begin at the inside corner with a direction normal to the hoop stress.

3.2 ELASTIC ANALYSIS

3.2.1 Geometry

The dimensions for the square plate with a nozzle are the same as the dimensions of the plate in previous chapters, except for the addition of a nozzle with thickness t_n and height of 1 inch. A plate with a symmetric nozzle is considered to investigate the effect of the nozzle on the stress concentration factor (SCF). The model for the finite element mesh is shown in Figure 3.6 and a schematic of the nozzle is shown in Figure 3.7.

3.2.2 Effect of Nozzle

In order to examine the effect of a nozzle, it is assumed that the nozzle extends symmetrically on both sides of the plate; this removes the effect of the bending that occurs if the nozzle is not symmetrical and it is desired to isolate the effect of the nozzle for SCF = 3. An asymmetry will cause local bending near the nozzle and affect the SCF.

With the nozzle in place, the geometric parameters are a, b, t, and the thickness of the nozzle is t_n . These parameters are divided by the plate thickness t, resulting in dimensionless ratios, a/t, b/t, and t_n/t. For a hole without the nozzle, $t_n = 0$, and the SCF is independent of a/t, provided b/t is large enough. Once the nozzle is added, the SCF varies with respect to two parameters, a/t and t_n /t.

Elastic analysis of the plate with a symmetric nozzle with an applied edge traction caused by in-plane forces in the far-field, determines the values for the SCF and the results are shown in Table 3.1 and Table 3.2; "Mises" is the maximum von Mises stress intensity, "Far" is the stress in the far-field, "EL#" is the number of the element where

the maximum stress is found, and "SCF" is the stress concentration factor obtained by dividing "Mises" by " Far". The results in Table 3.1 and Table 3.2 are determined employing the ABAQUS FE code and the KSHEL program. Also, high stresses are found at both the plate and the nozzle part.

According to the results in Table 3.1, even if the plate thickness is greater than the thickness of the nozzle, the nozzle stresses and calculated SCF value are greater than those of the plate. When the thicknesses of the plate and the nozzle are the same in magnitude, the SCF at the nozzle is also greater. For example, when the thickness of the plate, t, is 0.5 and the thickness of the nozzle, t_n, is 0.125, giving the ratio of thickness t_n /t = 0.25, the SCF at the nozzle is 3.456 and exceeds three. This indicates that in the nozzle, reverse yielding per cycle is produced. This special case will be treated later in detail employing plastic analysis.

In the plate, it is found that, depending on the plate and the nozzle wall thickness, these values lie between 1.242 and 2.158. The magnitudes of the elastic SCF for all cases do not exceed three; upon adding a nozzle, the maximum stress is reduced in comparison to that of the plate with a hole. This result indicates that the nozzle acts as a reinforcement to the plate. Table 3.2, including KSHEL results, also indicates similar results as Table 3.1.

The location of the maximum stress is also investigated. As shown in Table 3.1, when the thickness of the nozzle is increased, the maximum stress location moves from EL20 to EL10; when the nozzle thickness increases, the nozzle becomes a powerful reinforcement. The ABAQUS results indicate that at EL 1 in Figure 3.7, the longitudinal

compression with small tension in S11 occurs for a thin nozzle, while the longitudinal tension with large tension in S11 is produced for a thick nozzle. In other words, resisting force against compression increases as the thickness of the nozzle increases. For EL20, unlike EL 1, the resisting force against the traction increases. Therefore, the maximum compressive and tensile stresses can not be found at EL 1 or EL20, clearly shown in Figure 3.8 through 3.10, when comparing the results between the thin and the thick nozzle. Figure 3.8 displays the distribution of the S11 stress component and Figure 3.9 displays the distribution of the S22 stress component. In both figures, the location of the maximum stress of the S11 component and the location of the minimum stress of the S22 component of the thick nozzle, are found in the middle elements and not the end elements as expected. Correspondingly, the maximum stress intensity is found at the middle element, EL11 for the thick nozzle, as shown in Figure 3.10.

3.2.3 Results of Asymmetric Nozzle

The asymmetric nozzle model applied by the edge traction, is analyzed and the result is shown in Table 3.3. Compared to Table 3.1, all calculated values of the SCF in Table 3.2 are greater than those in Table 3.1. For a thin nozzle, the SCF at the plate approaches three, 2.793 to 2.938, and the SCF at the nozzle increases to 3.713; this indicates that the SCF is now affected by the bending resulting from the asymmetry of the nozzle.

The location of the highly stressed element is considered in this model. ABAQUS indicates that the highly stressed location is also affected by bending, as a

secondary effect of the traction. In the model for a symmetric nozzle, the location changes depending on the thickness of the nozzle, unlike the very thin nozzle where the thickness does not affect the location. However, in the present model, its location is consistent except for very thick nozzles, as shown in Table 3.3.

Even if there are some differences between the results from the analysis for the symmetric and the asymmetric nozzle, for both instances, the nozzle itself seems to act as a reinforcement to the plate. Moreover, because the thick nozzle is commonly used for constructing modern pressure vessels, it can be stated that the above result is worth further investigation.

3.3 PLASTIC ANALYSIS

Plastic analysis is performed to estimate the strain range for the case in which the SCF of the nozzle exceeds three and is highest at t = 0.5 and t_n = 0.125,. When the far-field stress is 26.67, the elastic solution indicates that the maximum stress intensity is 99.13 at the nozzle and 74.57 at the plate, confirming the SCF in Table 3.3. The equivalent elastic strains are calculated as E_{eq} = 0.00290 at the nozzle part and E_{eq} = 0.00257 at the plate part.

From plastic analysis, Figure 3.11 and 3.12 are obtained. The stress-strain history curve of Figure 3.11 indicates that, shakedown is achieved at both inside and outside surfaces of the plate for an in-plane force of 2Y/3. Capital letters in Figure 3.12, A through F, corresponds to those in Figure 3.11. For EL20 in the Plate, indicated in Figure 3.12, yielding starts at Point A and continues to Point C for a yield strength of

40.0. Unloading at EL20 follows the elastic curve in Figure 3.11, down to Point D without reverse yielding. It is seen in Figure 3.12 that Point D is placed below the line of the yield strength, Y = 40.0. For EL5019 in the nozzle, indicated in Figure 3.12, unloading at the inside surface of EL5019 follows the elastic slope up to Point D and then reverse yielding to Point E. The same pattern can be found for further cycles in the figure.

The cyclic equivalent strain range is calculated using equation (2-12), as E_{Range} = 0.00297 for the nozzle and E_{Range} = 0.00257 for the plate. The results indicate that the cyclic equivalent strain range at the plate under shakedown is equal to the equivalent strain range for the elastic solution. However, for the nozzle with reverse yielding, its value from the plastic solution is greater than that of the elastic solution, which indicates that the plastic strain is produced per cycle, at the nozzle parts, and results in the reduction of its lifetime. Here again, it is proven that accurate results are obtainable only through elastic-plastic analysis.

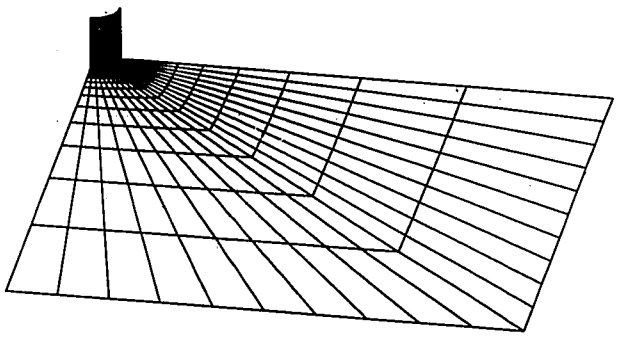

Figure 3.1 Finite Element Mesh for Square Plate with a Nozzle

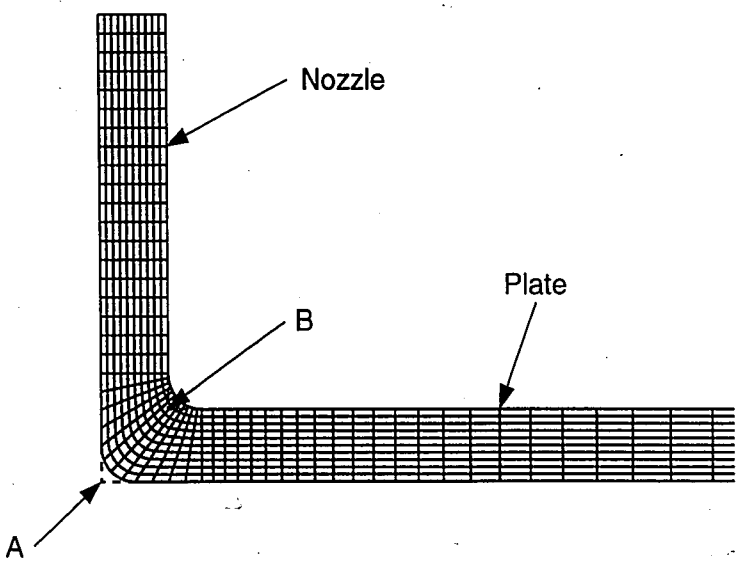

Figure 3.2 Finite Element Mesh for the Section of Square Plate with a Nozzle

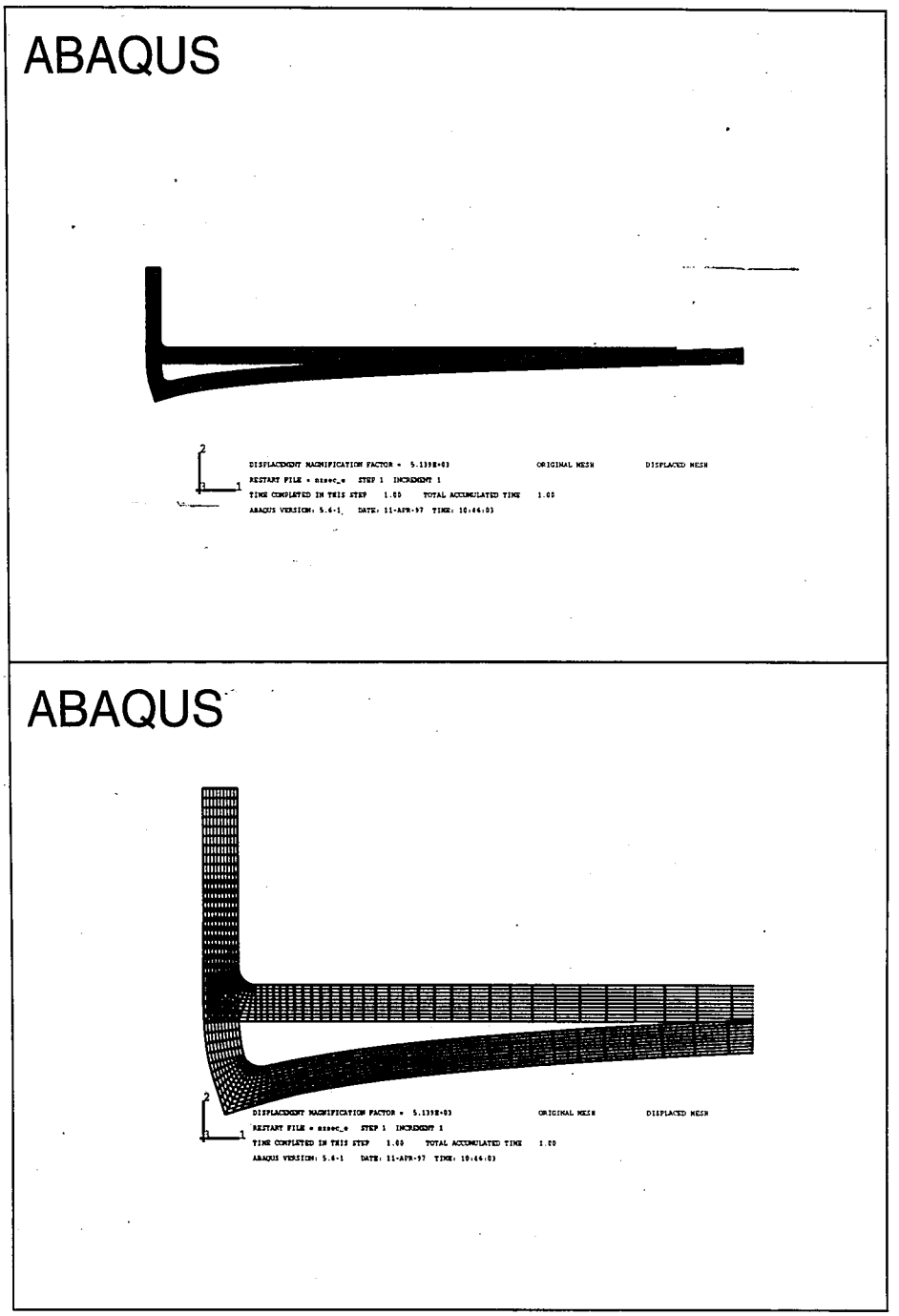

Figure 3.3 Deformed Shape of the Section of the Nozzle under Edge Traction

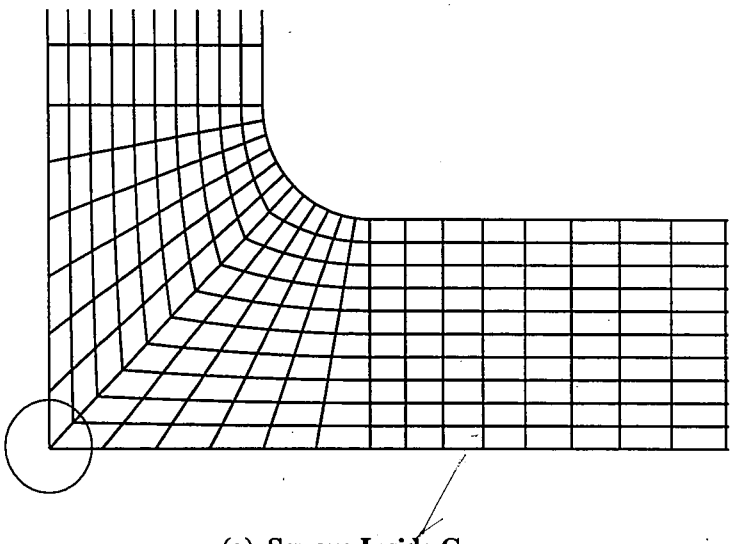

(a) Square Inside Corner

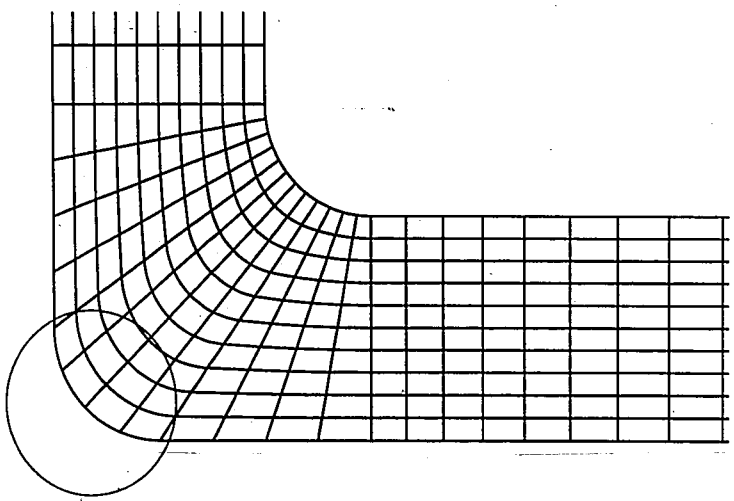

(b) Rounded Inside Corner

Figure 3.4 Section Models for Square-Edge Nozzle (a) and Rounded-Edge Nozzle (b)

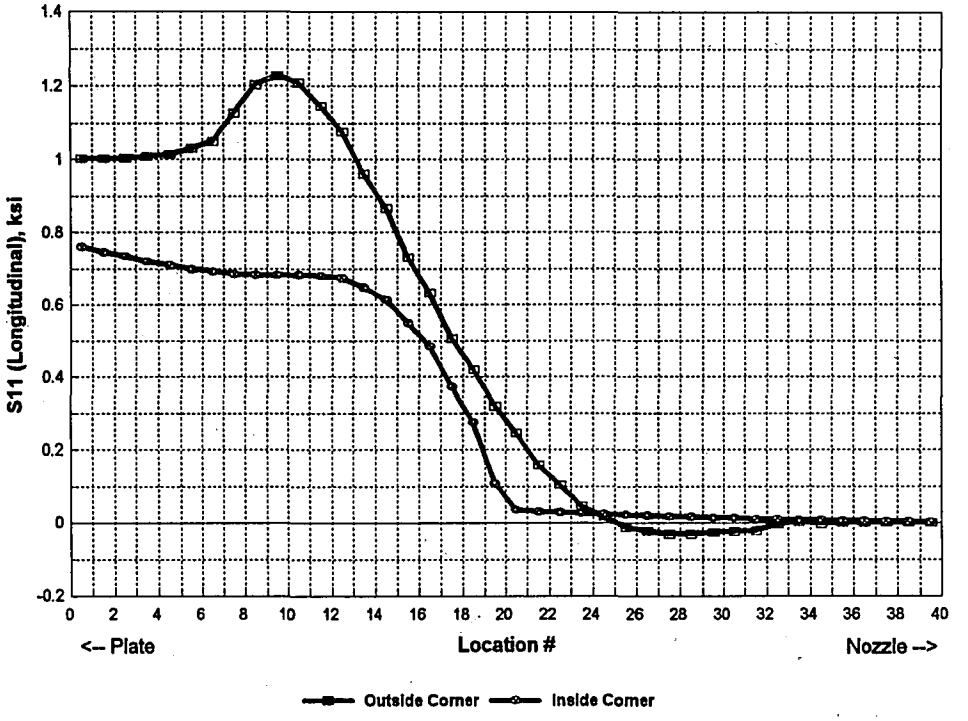

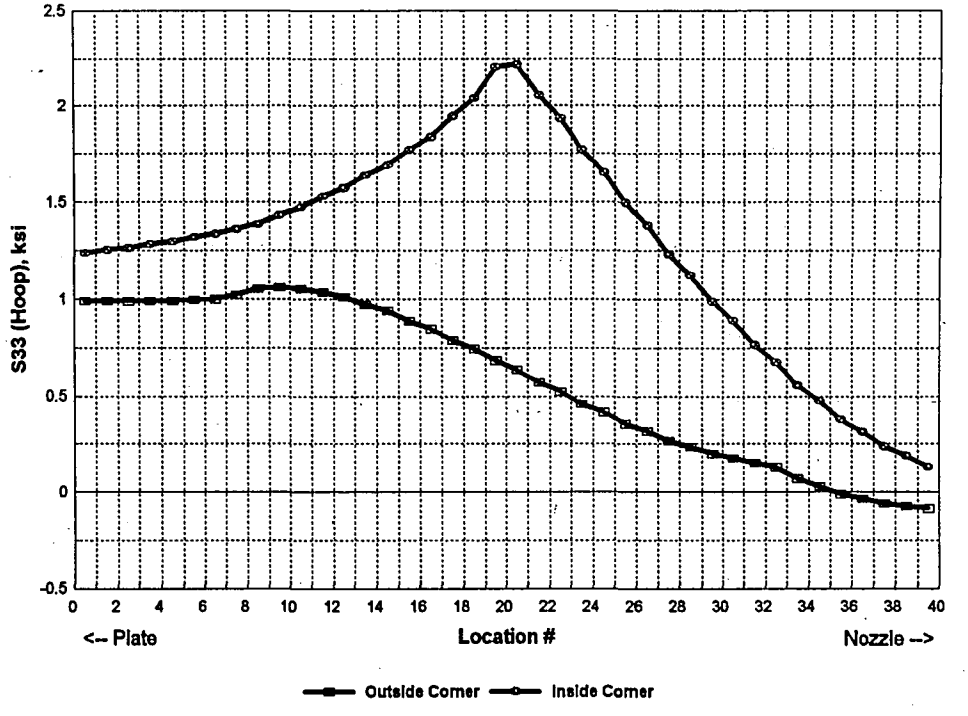

Figure 3.5 Distridutions of Stresses along Inside and Outside Corners for Square-Edge Nozzle

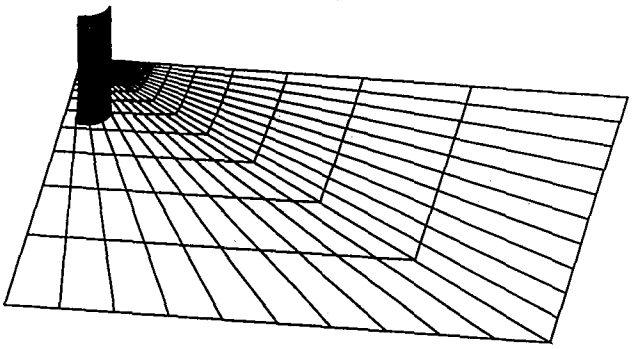

Figure 3.6 Finite Element Mesh for Square Plate with a Symmetric Nozzle

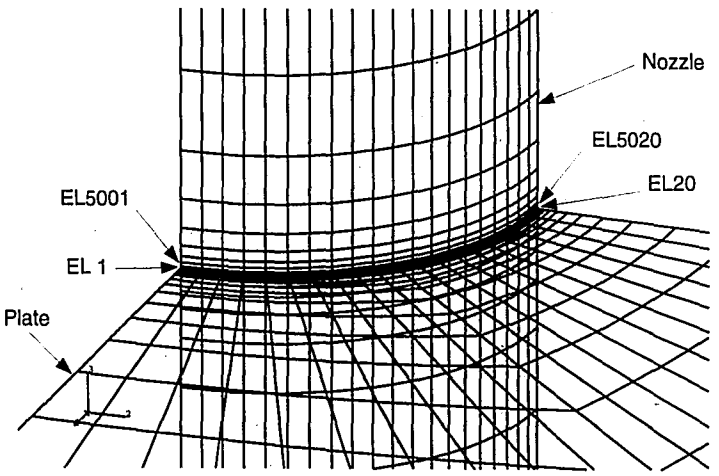

Figure 3.7 Finite Element Mesh near the Symmetric Nozzle

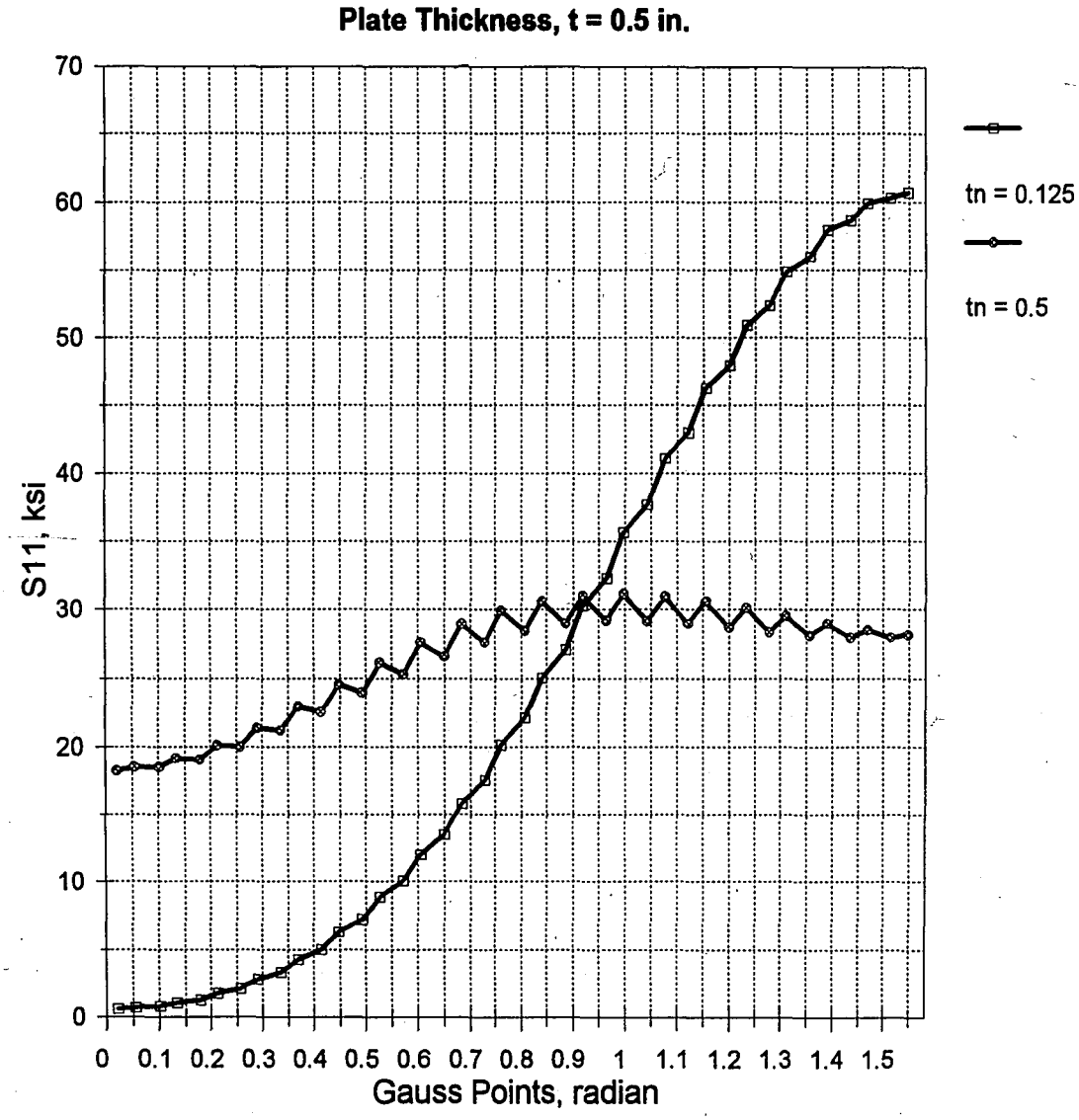

Figure 3.8 Distributions of S11 Stress Component around the Nozzle

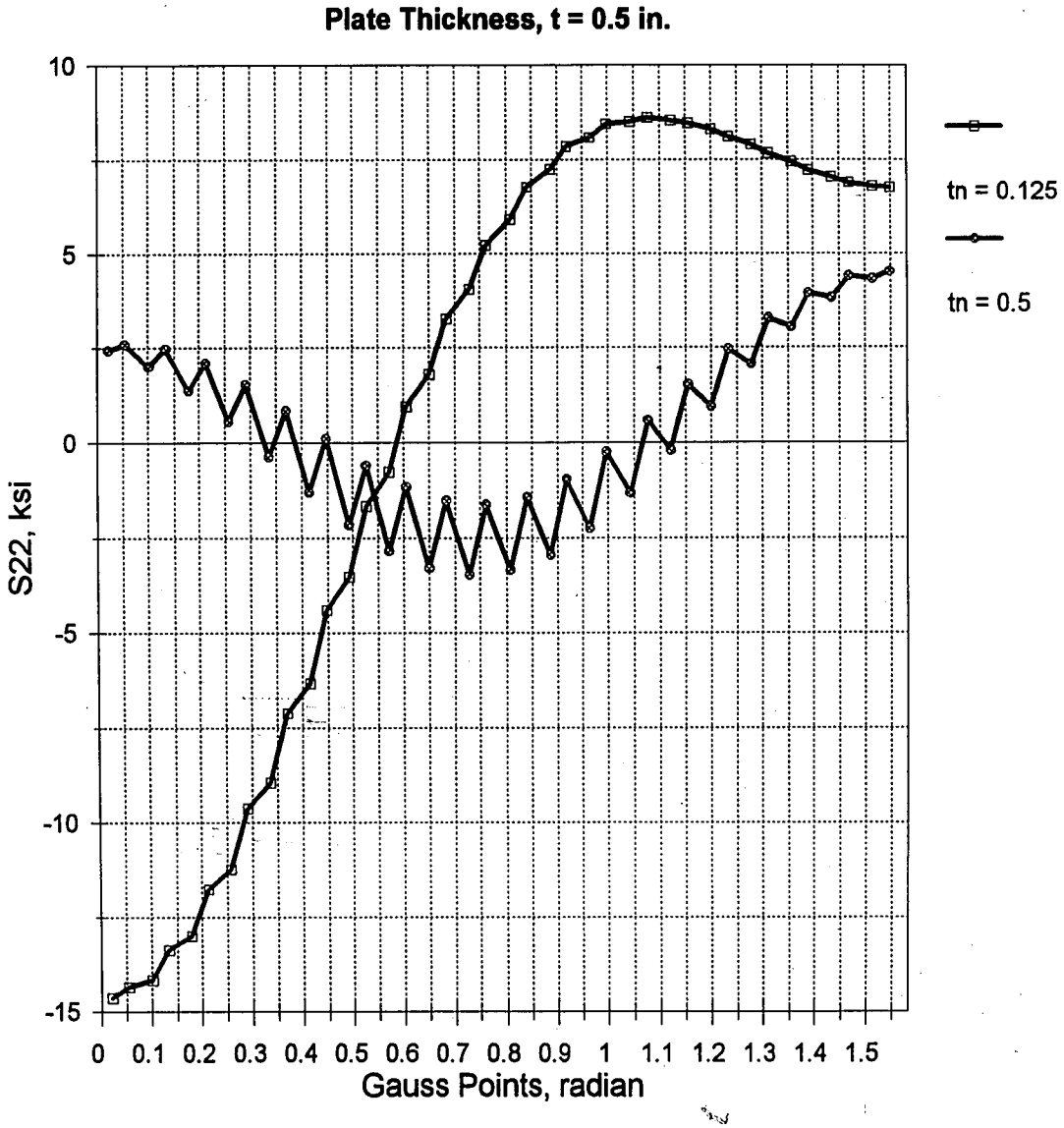

Figure 3.9 Distributions of S22 Stress Component around the Nozzle

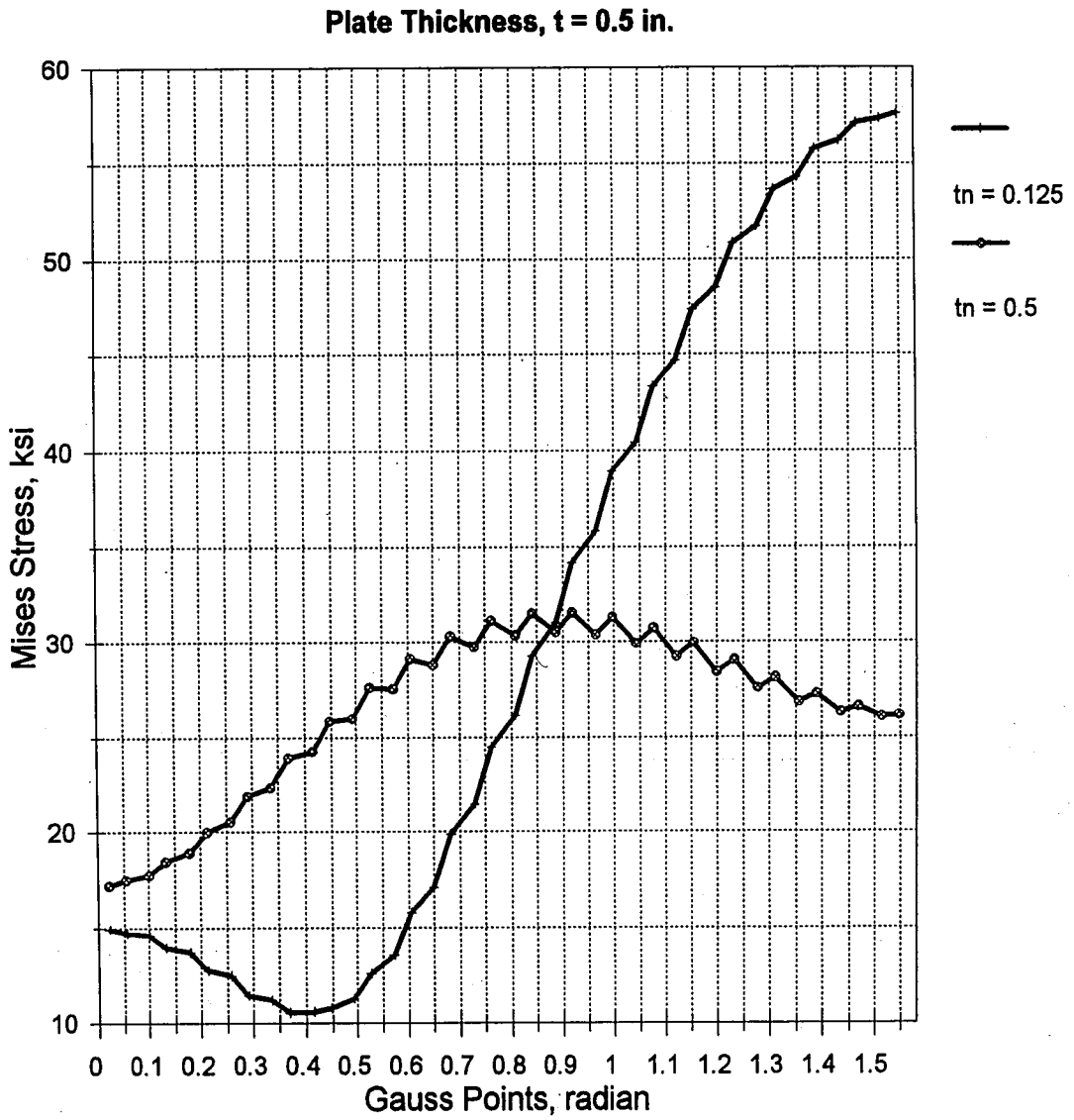

Figure 3.10 Distributions of von Mises Stress Intensity around the Nozzle

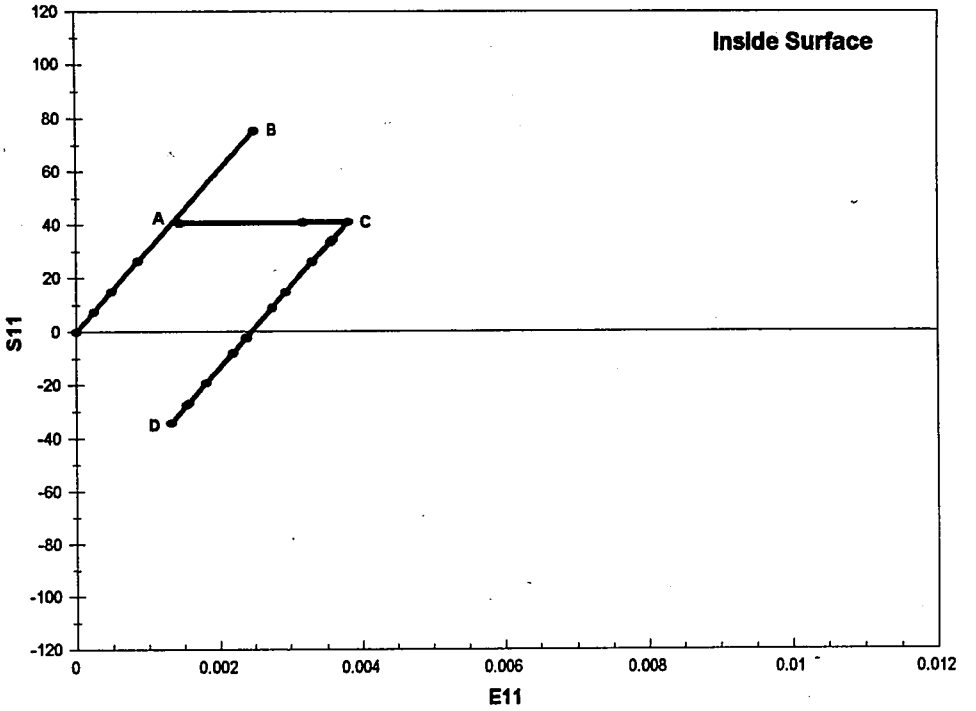

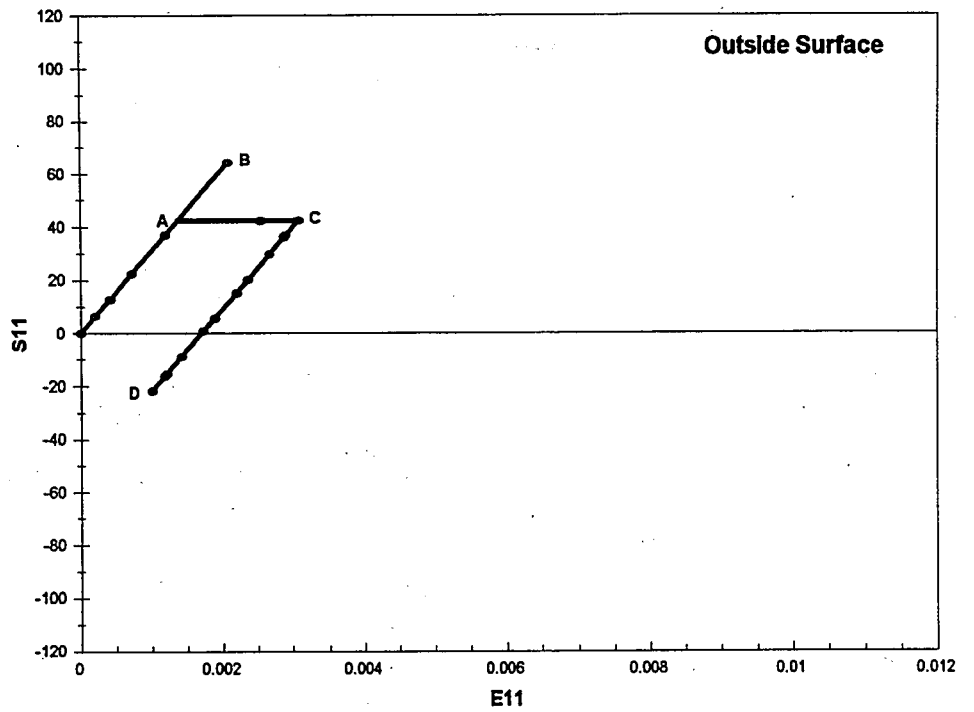

Figure 3.11 Stress-Strain Behavior at Most Strained Element in Nozzle Junction in Cycled Combined Load (Tension + Moment)

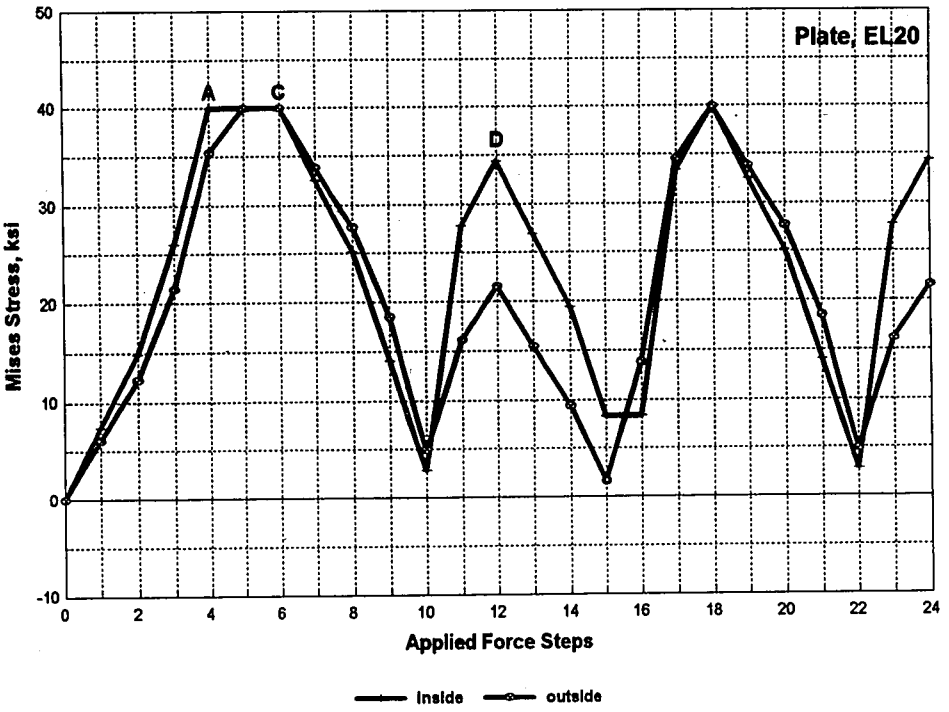

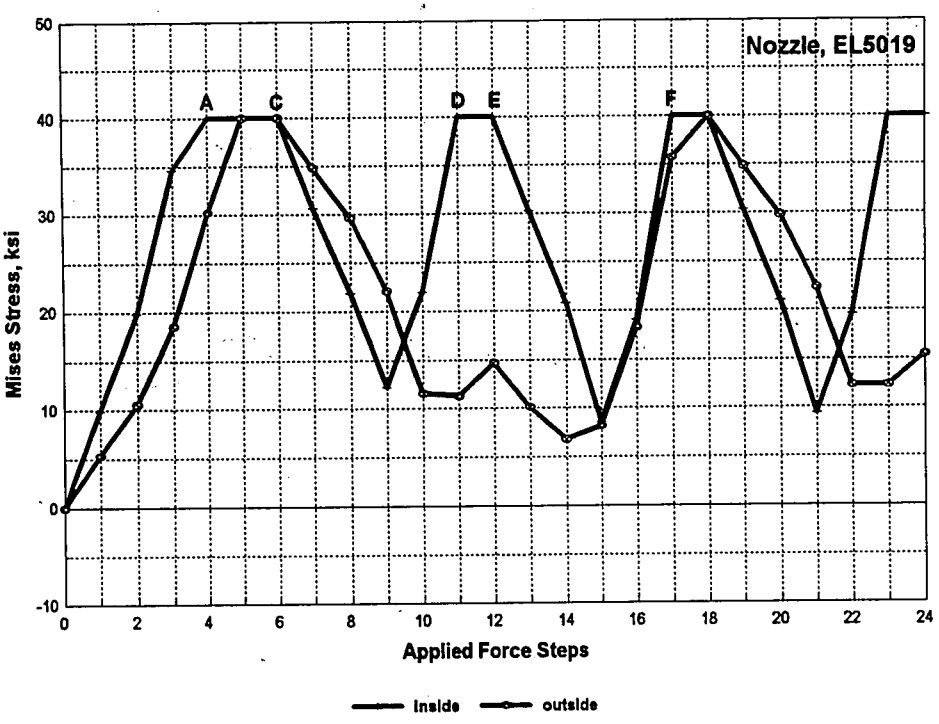

Figure 3.12 Von Mises Stress History at Most Strained Element in Nozzle Junction

Table 3.1 Elastic SCF in square plate with 1 in. diameter hole and symmetric nozzle using ABAQUS (Thicknesses in inches, Stresses in ksi)

t	tn	Mises (max)		EL#		Far	SCF	
		Plate	Nozzle	Plate	Nozzle	(Mises)	Plate	Nozzle
0.0625	0.0625	82.46	131.60	13	5020	53.37	1.545	2.466
0.0625	0.125	87.62	69.24	11	5020	53.35	1.642	1.298
0.125	0.0625	49.17	88.45	20	5020	26.69	1.842	3.314
0.125	0.125	40.07	53.41	12	5019	26.68	1.502	2.002
0.125	0.25	39.40	28.73	10	5019	26.67	1.477	1.077
0.25	0.125	22.54	37.03	20	5019	13.34	1.690	2.776
0.25	0.25	18.27	22.79	12	5019	13.34	1.370	1.708
0.25	0.375	18.02	15.89	10	5019	13.33	1.352	1.192
0.25	0.5	18.15	11.89	10	5019	13.34	1.361	0.891
0.375	0.125	17.56	28.41	20	5019	8.896	1.974	3.194
0.375	0.25	12.28	18.94	16	5019	8.893	1.381	2.130
0.375	0.375	11.43	13.91	12	5019	8.891	1.286	1.565
0.375	0.5	11.47	10.75	10	5019	8.889	1.290	1.209
0.5	0.125	14.40	23.06	20	5019	6.673	2.158	3.456
0.5	0.25	10.47	16.23	20	5019	6.671	1.569	2.433
0.5	0.375	8.52	12.37	14	5019	6.669	1.277	1.855
0.5	0.5	8.28	9.80	11	5019	6.668	1.242	1.470

Table 3.2 Elastic SCF in square plate with 1in. diameter hole and symmetric nozzle using KSHEL (Thicknesses in inches, Stresses in ksi)

t	tn	Mises (max)		Far	SCF	
		Plate	Nozzle	(Mises)	Plate	Nozzle
0.0625	0.0625	23.22	40.39	15.92	1.459	2.537
0.0625	0.125	24.82	20.56	15.96	1.555	1.288
0.125	0.0625	14.49	27.44	7.956	1.821	3.449
0.125	0.125	11.23	16.04	7.97	1.409	2.013
0.125	0.25	10.84	8.496	7.999	1.355	1.062
0.25	0.125	6.552	11.28	3.98	1.646	2.834
0.25	0.25	4.96	6.748	3.993	1.242	1.690
0.25	0.375	4.784	4.625	4.003	1.195	1.155
0.25	0.5	4.921	3.265	4.008	1.228	0.815
0.375	0.125	5.143	8.724	2.652	1.939	3.290
0.375	0.25	3.412	5.628	2.659	1.283	2.117
0.375	0.375	2.955	4.094	2.666	1.108	1.536
0.375	0.5	3.011	3.01	2.67	1.128	1.127
0.5	0.125	4.239	7.117	1.988	2.132	3.580
0.5	0.25	2.993	4.837	1.993	1.502	2.427
0.5	0.375	2.263	3.674	1.998	1.133	1.839
0.5	0.5	2.088	2.792	2.001	1.043	1.395

Table 3.3 Elastic SCF in square plate with 1in. diameter hole and asymmetric nozzle using ABAQUS (Thicknesses in inches, Stresses in ksi)

t	tn	Mises (max)		EL#		Far	SCF	
		Plate	Nozzle	Plate	Nozzle	(Mises)	Plate	Nozzle
0.0625	0.0625	132.70	133.30	20	5020	53.38	2.486	2.497
0.0625	0.125	87.92	103.40	18	5020	53.37	1.647	1.937
0.125	0.0625	78.45	84.01	20	5020	26.7	2.938	3.146
0.125	0.125	61.09	66.05	20	5020	26.69	2.289	2.475
0.125	0.25	40.99	49.61	17	5020	26.68	1.536	1.859
0.25	0.125	36.88	40.64	20	5020	13.35	2.763	3.044
0.25	0.25	28.46	32.55	20	5020	13.35	2.132	2.438
0.25	0.375	22.88	26.53	20	5020	13.34	1.715	1.989
0.25	0.5	19.58	21.77	17	5020	13.34	1.468	1.632
0.375	0.125	24.95	30.69	20	5020	8.899	2.804	3.449
0.375	0.25	21.48	24.61	20	5020	8.898	2.414	2.766
0.375	0.375	18.18	20.81	20	5020	8.896	2.044	2.339
0.375	0.5	15.77	17.68	20	5019	8.895	1.773	1.988
0.5	0.125	18.64	24.78	20	5019	6.674	2.793	3.713
0.5	0.25	16.80	20.04	20	5019	6.673	2.518	3.003
0.5	0.375	14.86	17.28	20	5019	6.673	2.227	2.590
0.5	0.5	13.24	14.98	20	5019	6.672	1.984	2.245

Chapter 4

ANALYSIS OF A TORISPHERICAL HEAD WITH A NOZZLE IN THE KNUCKLE

4.1 OVERVIEW

As stated in chapter 2, the knuckle of a torispherical head is under large compression, with a little bending in circumferential direction, and under tension, with inward bending in meridional direction. In this chapter, based on the results of the previous chapters, the torispherical head with a nozzle in the knuckle is analyzed. Before doing that, to get accurate results from ABAQUS FE code, the torispherical head without hole is examined and compared to the result of KSHEL program.

The modeling of torispherical head by using ABAQUS is not simple. Something can be neglected in the model and lead to wrong results. Therefore, verification of the finite element model is one of the most important steps in finite element analysis. Here is a way to get rid of this kind of inconsistency, which is found as modeling the head.

Finally, the elastic SCF of a torispherical head with a nozzle in the knuckle with respect to various thickness ratio, t_n /t, from which shakedown can be estimated, is suggested for vessel design.

4.2 GEOMETRY

A torispherical head is selected with r = 3.6, D = L = 60, all in inches, where r is the radius of torus, D is the diameter of cylinder, and L is the radius of sphere. A hole of radius a = 0.5 is cut out in the middle of the knuckle. The circle of the midsurface at the end of a nozzle is attached to the circle of the midsurface of the hole. The nozzle is protruding out of the head only.

4.2.1 Finite Element Modeling

Shell elements of the ABAQUS FE code, S8R, are employed for modeling the head consisting a sector of the head. To construct three-dimensional finite element model, MAP function provided by ABAQUS is effectively used here[12]. For each of the parts, the head, sphere, torus, and cylinder, the types of MAP function are exactly matched to those parts. But, nodes mapped by TOROIDAL type, which is one of the options for MAP function, have a different coordinate system from nodes by mapping using both SPHERICAL and CYLINDRICAL options. This difference affects the orientation of element properties and can result in wrong calculated stresses, strains, and all output related to elements, even plot results at post-processing. Therefore, it is very important to get rid of this inconsistency from ABAQUS mapping. The way to do so and to get a correct result from analysis is to add the ORIENTATION card to the ABAQUS input file.

The finite element model of the head without a hole is shown in Figure 4.1 and the head with nozzle in Figure 4.2, describing the number of noticeable nodes and elements. A detail of the nozzle and the knuckle is also shown in Figure 4.3 and 4.4, respectively.

4.2.2 Load and Boundary Conditions

A pressure of 1 psi is applied for analysis to get useful data for calculating the shakedown pressure of the head under cyclic loading. The pressure is applied to the inside surface of the head and no pressure is applied to the nozzle. The boundary conditions are those of symmetry in θ direction along two meridional edges, applied to node numbers N1 to N6801 and N21 to N6821 in Figure 4.1 and the restraint in Z-direction along the bottom edge of the cylindrical parts, N1 to N21.

4.3 RESULTS OF ANALYSIS

4.3.1 The Head without Hole

The elastic analysis can estimates whether or not the finite element model being used is reasonable and is compatible with the theory of elasticity, using the head with no hole shown in Figure 4.1.

According to the theory of plates and shells [16], for the toroidal parts, the membrane forces, N_φ and N_θ, are given by:

$$N_{\varphi} = \frac{p\left(r_0^{\,2} - r_a^{\,2}\right)}{2r_0 \sin\varphi} \quad \text{----------} \quad (4\text{-}1)$$

$$N_{\theta} = \frac{pr_a}{2} \quad \text{----------} \quad (4\text{-}2)$$

where p = uniform pressure

r_0 = radius of a parallel circle on a torus

r_a = radius of a circle

φ = angle

For the cylindrical parts,

$$N_{\varphi} = \frac{pr_a}{2} \quad \text{----------} \quad (4\text{-}3)$$

$$N_{\theta} = pr_a \quad \text{----------} \quad (4\text{-}4)$$

where r_a = radius of a cylinder

For the spherical parts,

$$N_{\varphi} = N_{\theta} = \frac{pr_a}{2} \quad \text{----------} \quad (4\text{-}5)$$

where r_a = radius of a sphere

By employing these equations, all membrane forces of the head without hole can be obtained when three parts are not jointed each other. ABAQUS calculates the same magnitudes of each membrane forces as the above equations for the finite element model of spherical and cylinderical parts shown in Figure 4.1. In other words, it indicates that the finite element model in Figure 4.1 is acceptable for further analyses. It is impossible to calculate the membrane forces of toroidal parts by the above equations when three

parts are jointed. The reason is that bending stresses arise at the parts having a function of a connector between the sphere and the cylinder. Results can be obtained by running computer codes such as KSHEL or ABAQUS.

The maximum element force for t = 0.125 is found at the middle of meridional edge in the toroidal parts of the head and has $N_\theta = -133.6$. At this location, $N_\varphi = 18.81$, $M_\theta = -0.6445$, and $M_\varphi = -2.149$. KSHEL program calculates $N_\theta = -133.6$, $N_\varphi = 18.98$, $M_\theta = -0.6562$, and $M_\varphi = -2.195$. The KSHEL result indicates that the maximum force is the same as the ABAQUS result and the other are similar. These values are employed for comparing to the values of a far-field element of the head with nozzle. The deformed shape of the head without a hole is shown in Figure 4.5, and the distribution of element forces, N_φ and N_θ, and the von Mises stress intensity on the inside and outside surfaces is plotted along the meridian of the head in Figure 4.6 and 4.7.

4.3.2 The Head with Nozzle

The strain range is now calculated by an elastic analysis that neglects the effect of the deformed geometry. For a pressure of 1 psi, the maximum von Mises stress intensity at two locations, near the nozzle and in the far-field on the same latitude circle as that of the center of the nozzle, are calculated by ABAQUS. The results are shown in Table 4.1 and the table headings are the same as those of Table 3.1. From the results of Table 4.1, when the nozzle is neglected, $t_n = 0$, the SCF is 2.795 in the head. But, if the nozzle is

added, all calculated SCF on the head are lower than 2.795 and have the value between 1.359 and 2.149. It confirms again that the nozzle acts as a reinforcement to the head.

The results of Table 4.1 can be employed for estimating the number of cycles to fatigue failure and for calculating the shakedown pressure for the head. For example, if Fig. 5-110.1 of Division 2, Section VIII, of the ASME (1995) B&PV Code is used, then the alternating stress required for the ordinate of this figure is given by the cyclic pressure times the numbers in the column "Head" under "Mises (max)", divided by 2. For a cyclic pressure of 80 psi for the head with t = 0.125 and t_n = 0.125, the alternating stress σ_{alt} is given by

$$\sigma_{alt} = 80 \times 2.976 / 2 = 119.04 \text{ ksi} \quad \text{----------(4-6)}$$

Since this number comes from the strain range times the modulus of elasticity, E = 30,000, divided by 2, the corresponding strain range is predicted by elastic analysis as

$$E_{Range} = 80 \times 2.976 / 30{,}000 = 0.00794 \quad \text{----------(4-7)}$$

For given cyclic pressures for the other head geometry, the strain ranges can be calculated from the results of Table 4.1. In addition, if yield strength of a material, Y, is known, shakedown pressure of a head can be calculated by using the table. For example, when yield strength of the head with t = 0.125 and t_n = 0.125 is 40.0 ksi, then shakedown pressure is given by

$$P_{sk} = 2 \times 40 / 2.976 = 26.88 \text{ psi} \quad \text{----------(4-8)}$$

The SCF in a thin nozzle is near three, as listed in Table 4.1. These are bending stresses that come from the ovaling of the nozzle.

The distribution of the von Mises stress intensity on the inside and outside surfaces about various thickness ratio is plotted along the rim of the hole in Figure 4.8 when t = 0.125 and in Figure 4.9 when t = 0.25. These two figures indicate that the maximum stress intensity is found at the inside surface of EL2020 in Figure 4.4, near to the apex of the head. It is determined that, when t = 0.125, the maximum stress intensity decreases, according as the thickness of the nozzle increases, while, when t = 0.25, the maximum stress intensity increases, according as the thickness of the nozzle increases. The deformed shapes of the head with nozzle are shown in Figure 4.10.

The elastic-plastic analysis is not performed for the head in this thesis. But, according to the results shown in [20], due to the substantial effect of the geometric strengthening, the strain range obtained from an elastic-plastic analysis is far smaller than the range predicted by an elastic analysis. This result suggests again that the pursuit of plastic analysis may be worthwhile to produce more economical designs.

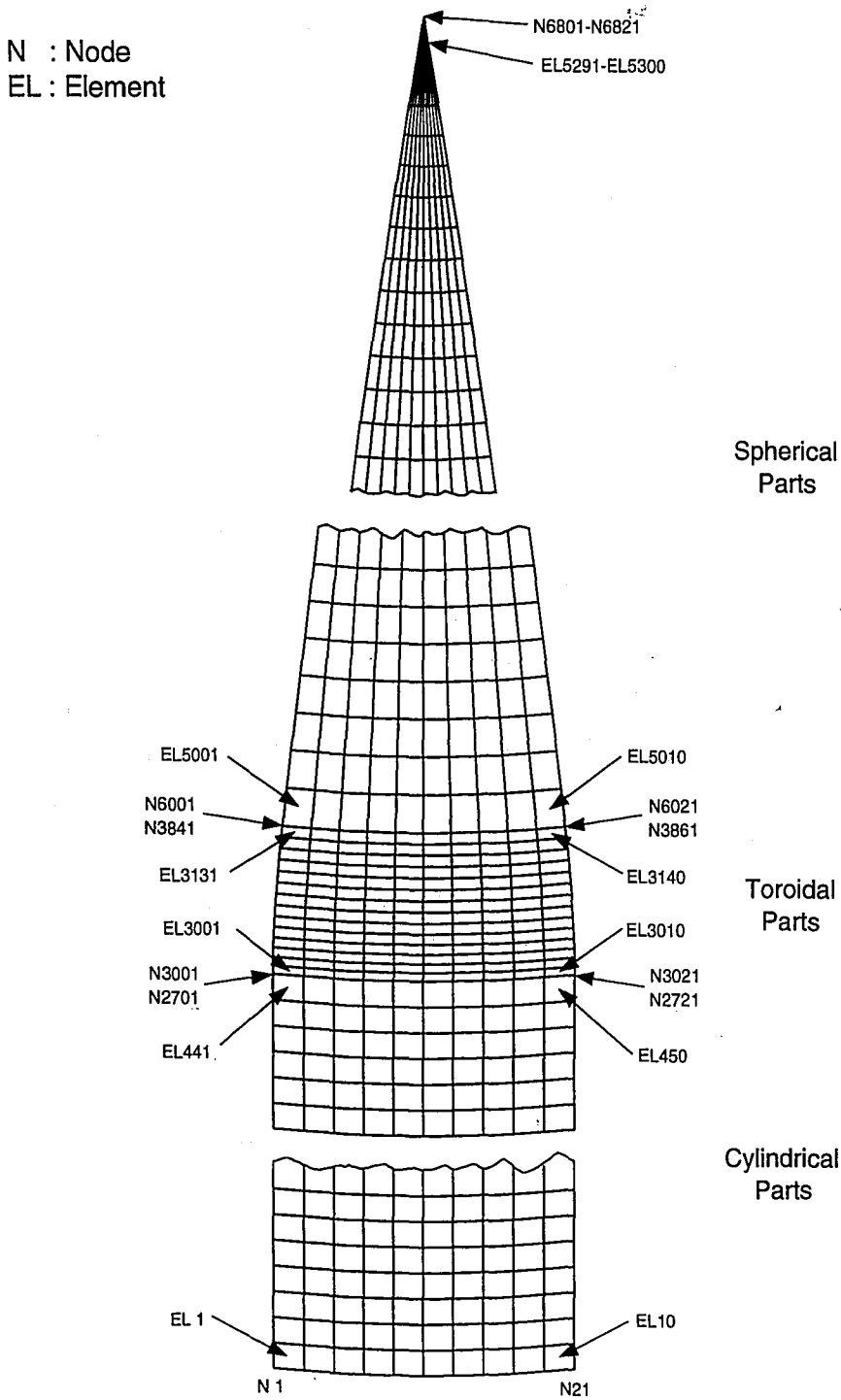

Figure 4.1 Finite Element Mesh for Torispherical Head without Hole at the Knuckle

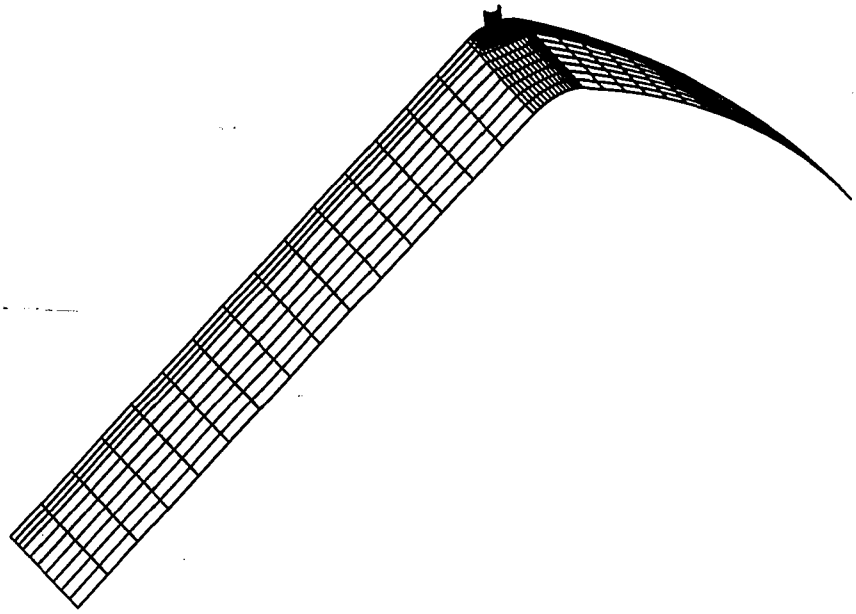

Figure 4.2 Finite Element Mesh for Torispherical Head with a Nozzle at the Knuckle

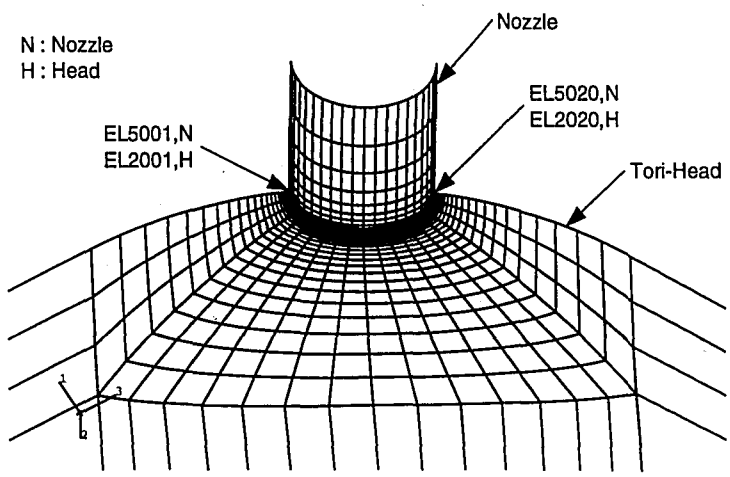

Figure 4.3 Finite Element Mesh near the Nozzle

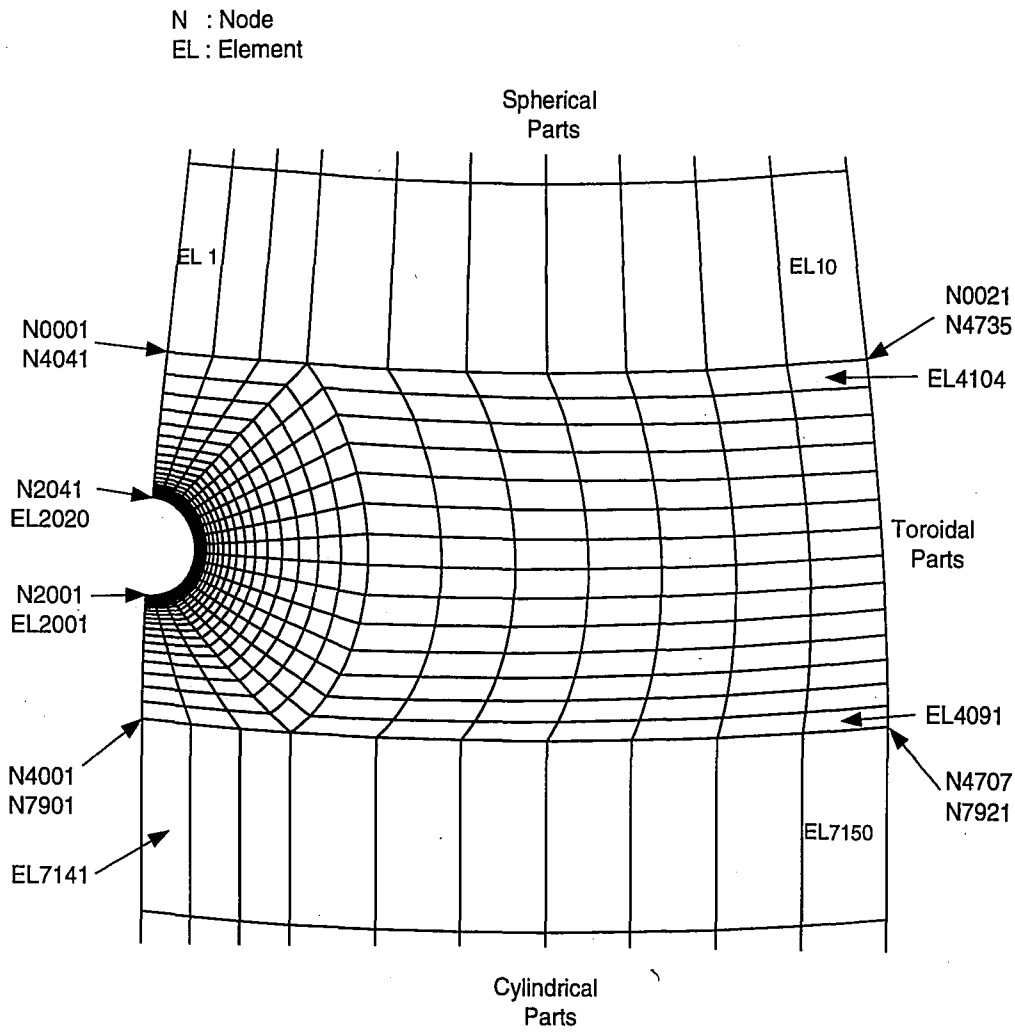

Figure 4.4 Finite Element Mesh near the Knuckle

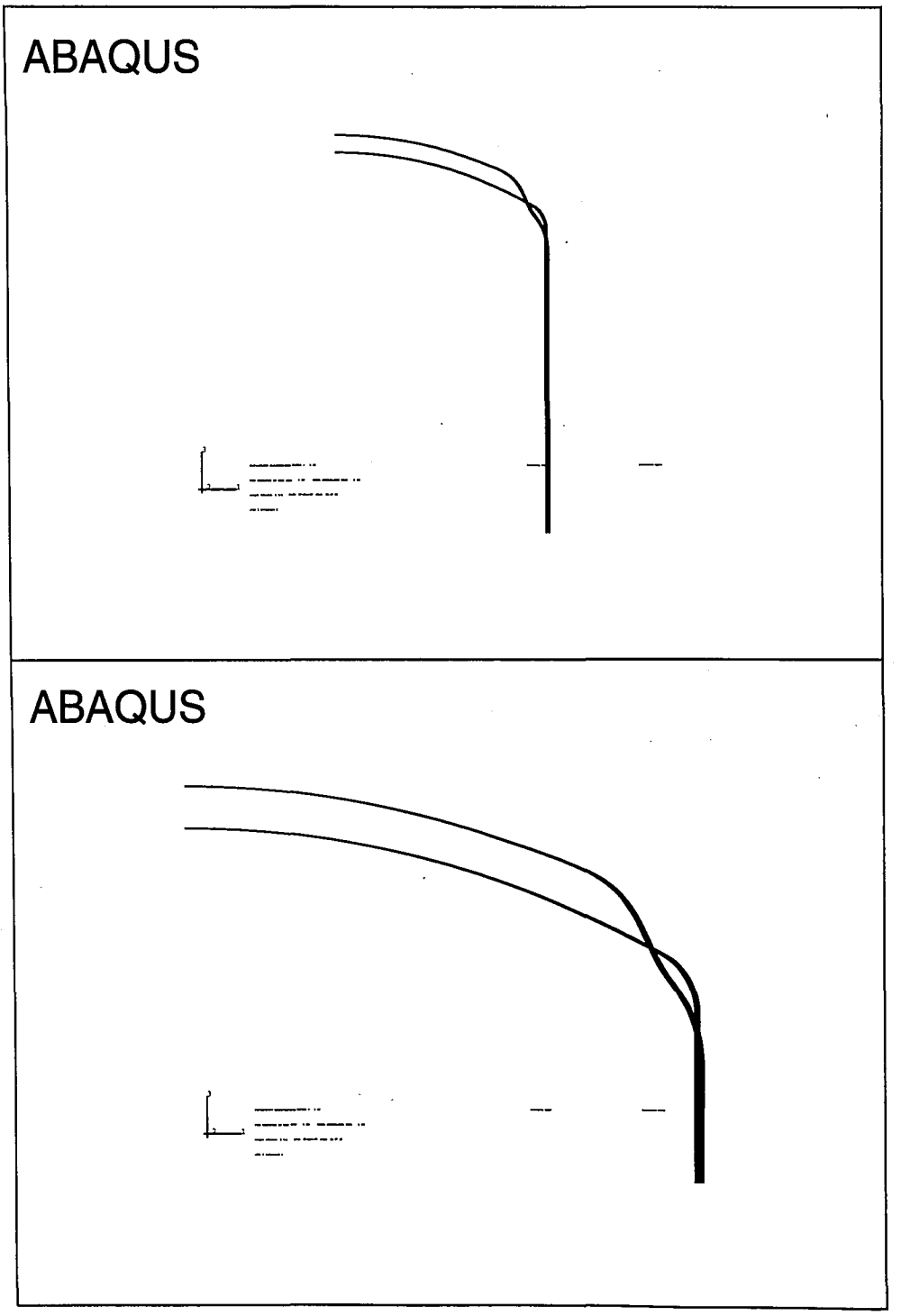

Figure 4.5 Deformed Shape of Torospherical Head without a Nozzle at the Knuckle

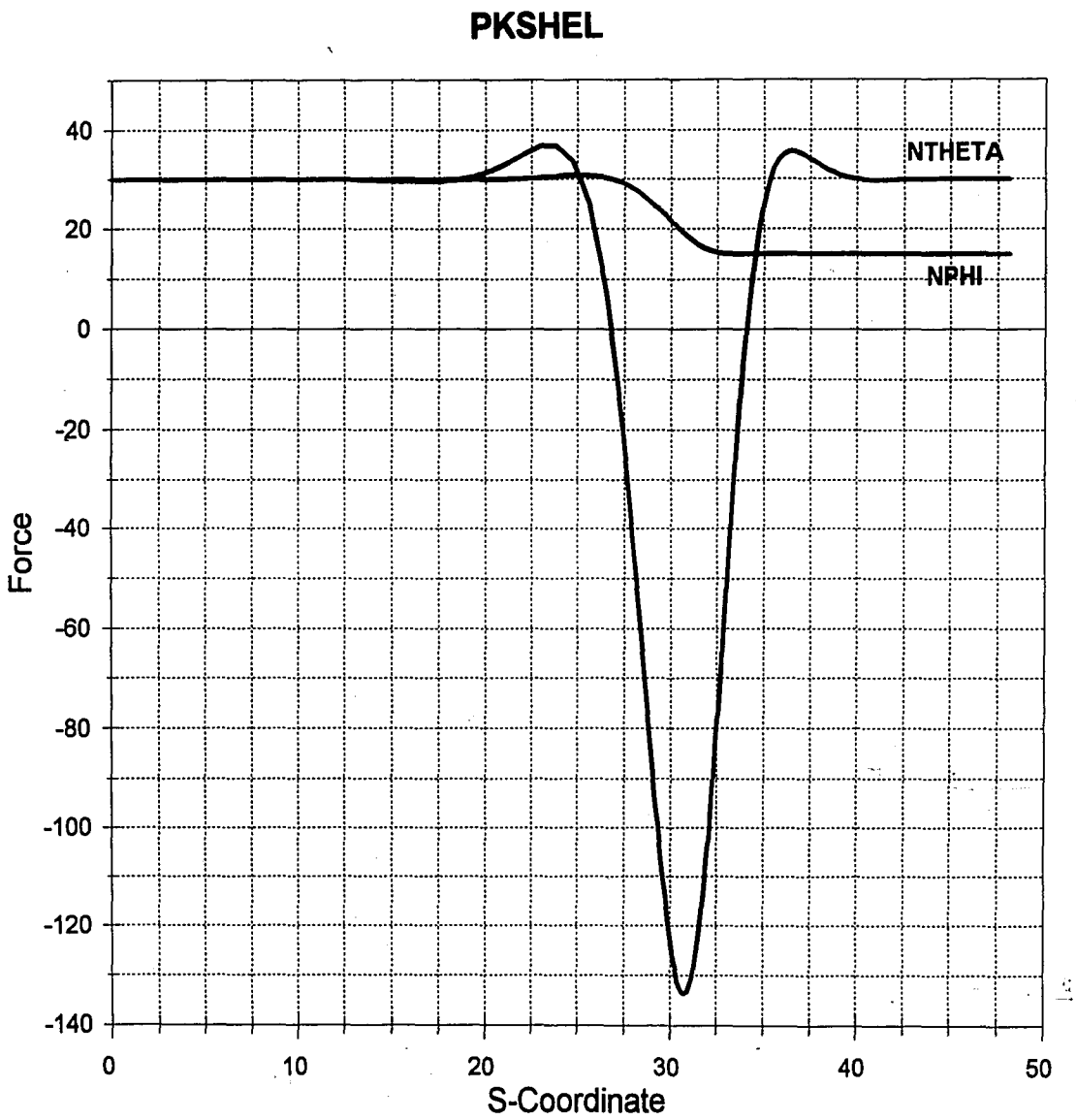

Figure 4.6 Distribution of Element Forces of Torispherical Head without a Nozzle along Meridian

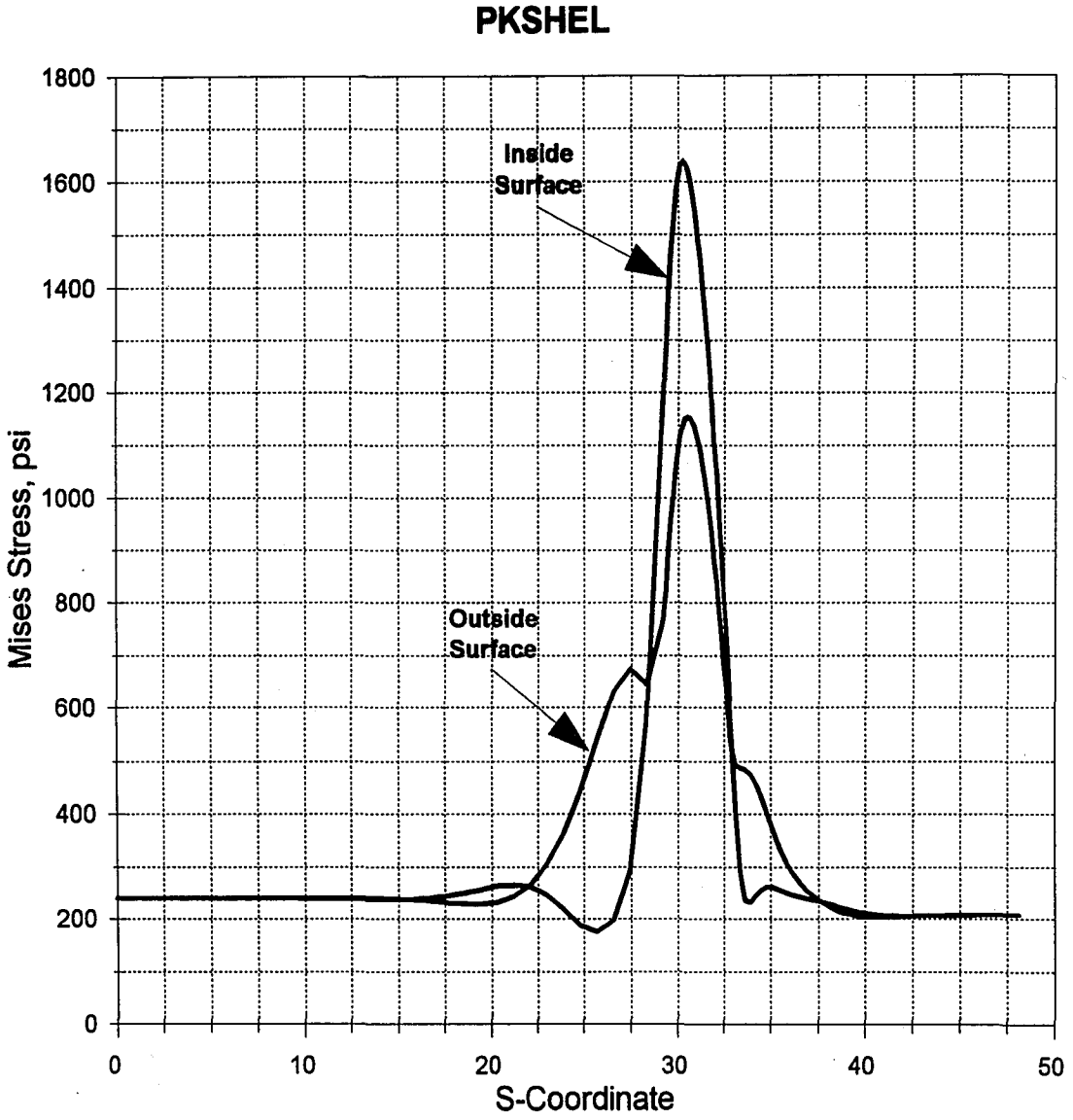

Figure 4.7 Distribution of von Mises Stress Intensity of Torispherical Head without a Nozzle along Meridian

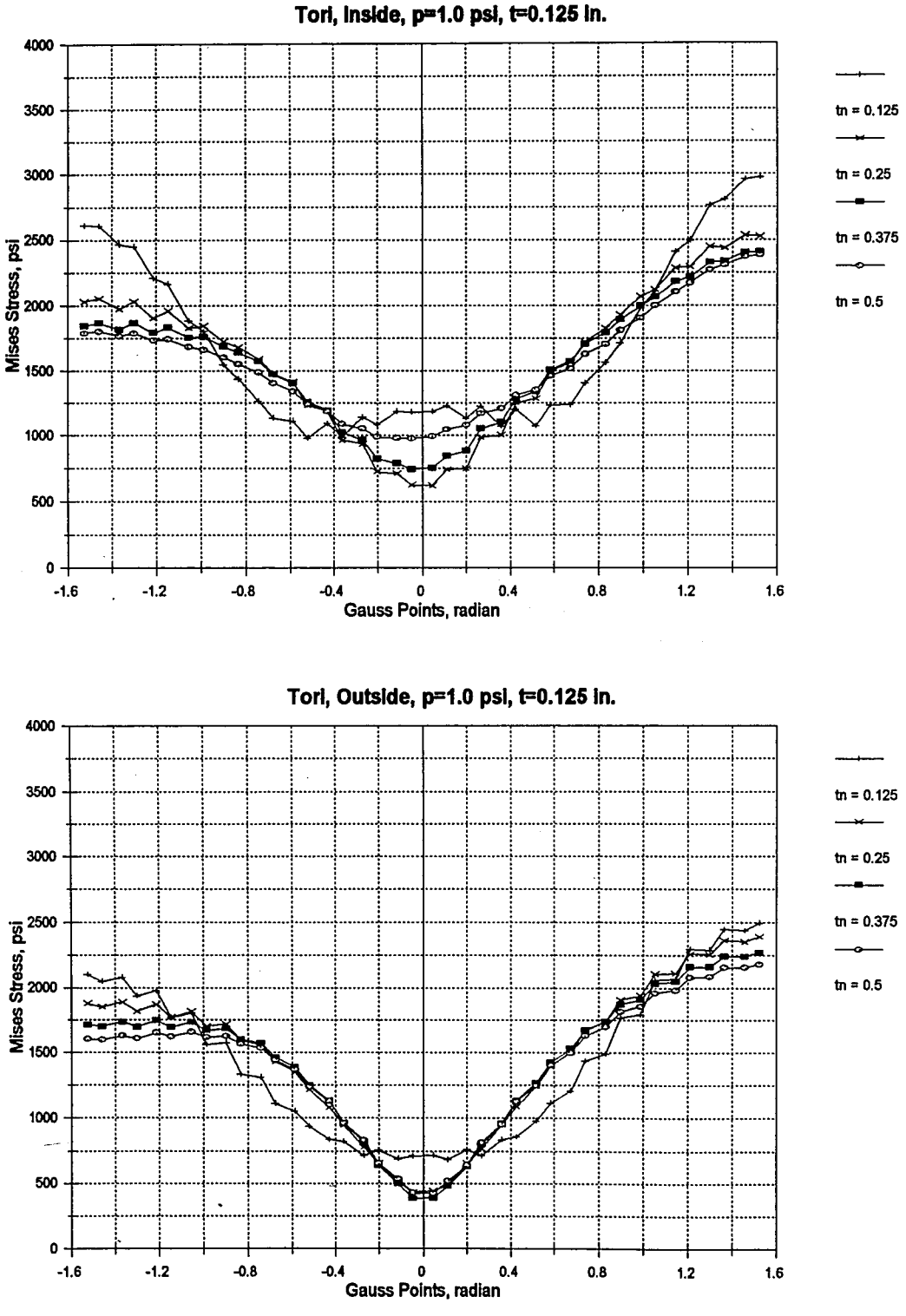

Figure 4.8 Distributions of von Mises Stress Intensity around Nozzle Junction When t = 0.125 inches.

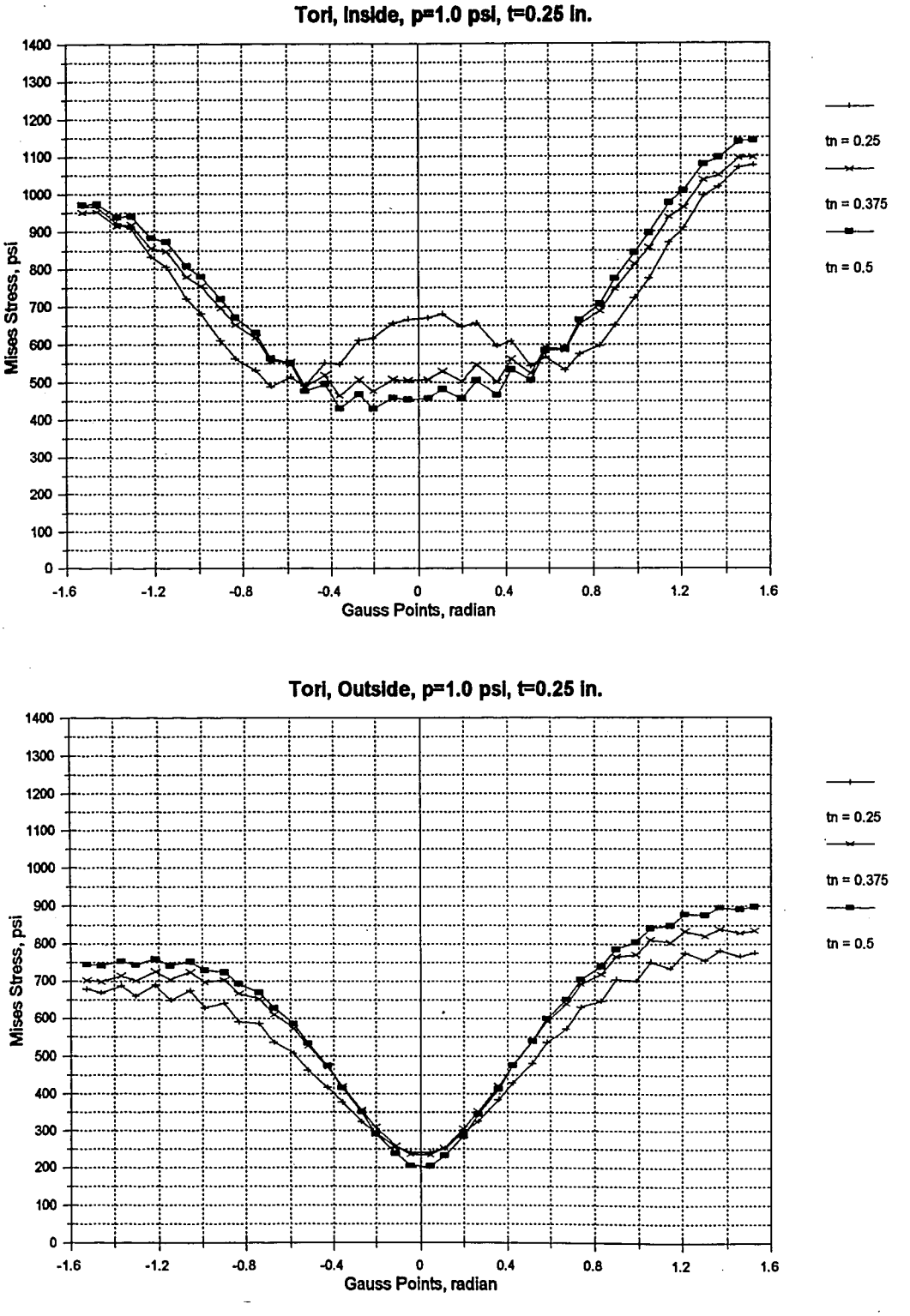

Figure 4.9 Distributions of von Mises Stress Intensity around Nozzle Junction When t = 0.25 inches.

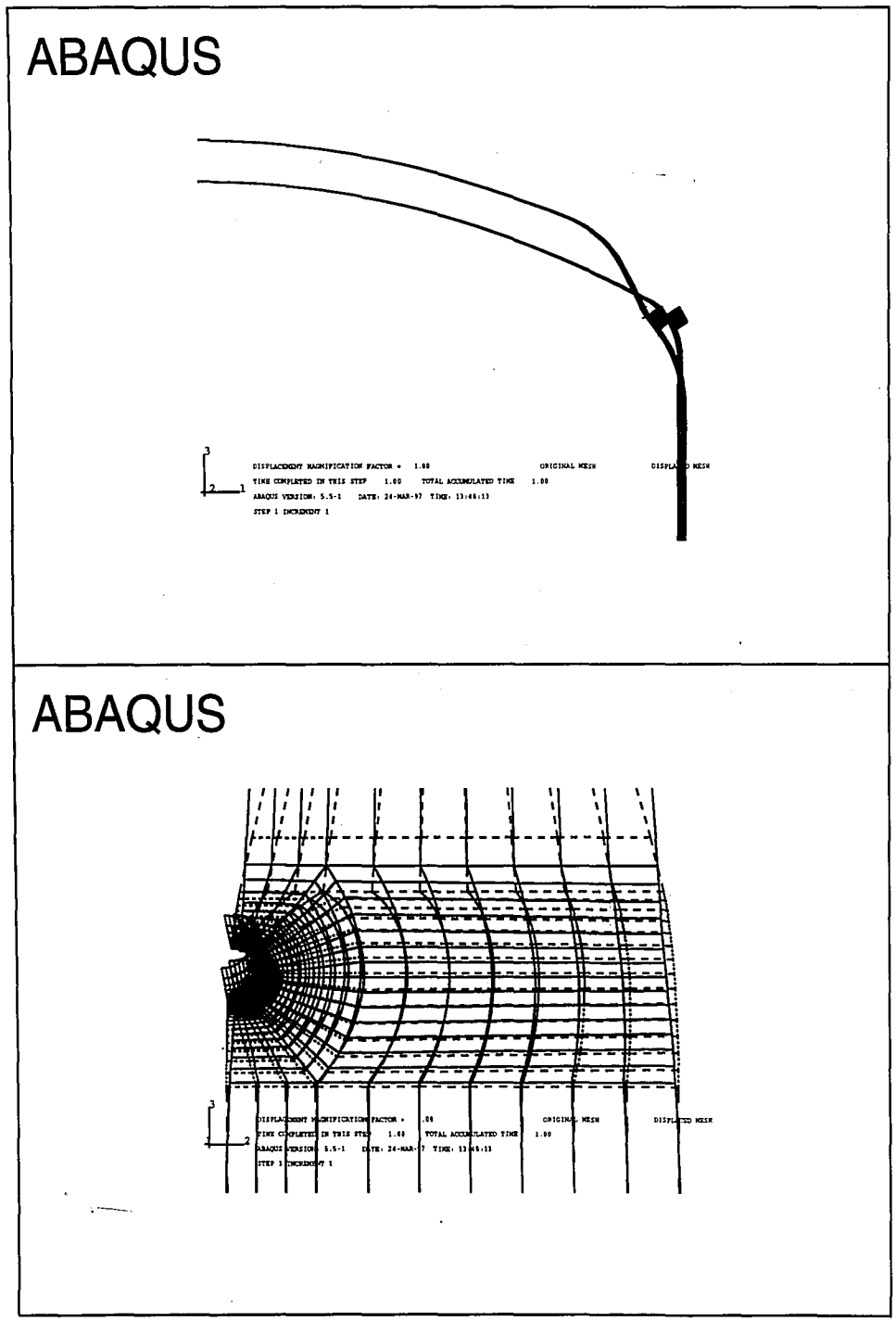

Figure 4.10 Deformed Shape of Torispherical Head with a Nozzle at the Knuckle

Table 4.1 Elastic SCF in torispherical head with 1in. diameter hole and nozzle (Thicknesses in inches, Stresses in ksi)

t	tn	Mises (max)		EL#		Far	SCF	
		Head	Nozzle	Head	Nozzle	(Mises)	Head	Nozzle
0.125		4.128		2020		1.477	2.795	
0.125	0.125	2.976	3.412	2020	5020	1.472	2.022	2.318
0.125	0.25	2.533	2.138	2020	5020	1.471	1.722	1.453
0.25	0.125	1.097	1.852	2020	5020	0.6757	1.624	2.741
0.25	0.25	1.076	1.221	2020	5020	0.6744	1.595	1.810
0.25	0.375	1.096	0.9043	2020	5020	0.6736	1.627	1.342
0.25	0.5	1.142	0.6972	2020	5020	0.6731	1.697	1.036
0.375	0.125	0.8882	1.119	2011	5020	0.4134	2.149	2.707
0.375	0.25	0.5971	0.8181	2011	5020	0.4124	1.448	1.984
0.375	0.375	0.5967	0.6305	2020	5020	0.4117	1.449	1.531
0.375	0.5	0.6377	0.5006	2020	5020	0.4112	1.551	1.217
0.5	0.125	0.5904	0.7387	2011	5020	0.2877	2.052	2.568
0.5	0.25	0.4999	0.5829	2011	5020	0.2871	1.741	2.030
0.5	0.375	0.4248	0.4695	2011	5020	0.2866	1.482	1.638
0.5	0.5	0.3889	0.3833	2020	5020	0.2862	1.359	1.339

Chapter 5

CONCLUSIONS

Finite element method is widely used in current engineering practice to analyze complicated geometries. By using this method, all results in this thesis were obtained. The ABAQUS FE code was used to analyze simple and complicated models. From analyzing a simple model, the square plate with a hole and a nozzle, the following results were obtained:

1) The ABAQUS element S8R is the appropriate element for modeling the geometries considered in this thesis because the effect of transverse shearing is needed in the plastic analysis.

2) If the primary stress field is limited to two thirds of the yield strength, shakedown is ensured for a SCF not exceeding three.

3) When plastic action occurs, the strain concentration factor (ECF) is greater than the elastic stress concentration factor (SCF) for a hole without nozzle. This means that the strain range calculated by elastic analysis is unconservative if shakedown does not occur. Thus, the use of an elastic-plastic large deflection analysis can lead to a more economical design of a structure than an elastic analysis.

4) The cyclic strain range can be easily calculated by multiplying the yield strength in a ABAQUS input file by two.

5) In plastic region, when the far-field stress is reduced back to zero after first yielding, the strain range should be considered as an important factor instead of the stress and strain concentration factors (SCF, ECF) because the calculation of those factors at unloading step is meaningless.

6) When combined in-plane forces and moments are applied along an edge of the square plate with a hole, the SCF is reduced by 22.7 to 50.7 percent.

7) From analyzing the axisymmetric model of the plate with a nozzle, it is determined that the maximum stress is the hoop stress and its magnitude at the inside corner is greater than that of the outside corner.

8) When a thick nozzle is attached to the plate, the location of the maximum stress is moved from the end of the hole to the middle.

9) A nozzle can lower the elastic SCF considerably.

These results are presented for the relatively simple model of a square plate. They are useful for a comparison with the much more complicated model of a nozzle in the knuckle of a torispherical head. The major difference between the head and the plate is that the head strengthens as it deforms while the plate does not. Another difference is that, if designed by plastic analysis, the stresses around the nozzle in the knuckle of a head are not subjected to specific stress limits.

And, from analyses of the torispherical head with a nozzle in the knuckle, the conclusions were the following:

10) If TOROIDAL MAP function of ABAQUS is employed to make the finite element mesh of a geometry, the ORIENTATION card should be added to the ABAQUS input file to get a correct result from the analysis.

11) The elastic stress concentration factor (SCF) is decreased by an increase in the nozzle thickness (hole size remaining the same), which is expected by the reinforcement that the nozzle provides to an unreinforced hole. Therefore, the results in Table 4.1 can be used in estimating the stress concentration factor. It is concluded that an assumed SCF = 3 overestimates the stress significantly.

REFERENCES

1. Nichols, R.W., "Pressure Vessel Engineering Technology," Elsevier Publishing Company Limited, Amsterdam-London-New York, 1971, Chapter 2.
2. Peterson, R.E., "Stress Concentration Factors," John Wiley & Sons, Inc., 1974.
3. Timoshenko, S.P., Goodier, J.N., "Theory of Elasticity," 3rd Edition, McGraw-Hill Book Company, 1970.
4. Savin, G.N., "Stress Concentration around Holes," Pergamon Press, 1961.
5. Raymond J. Roark, Warren C. Young, "Formulas for Stress and Strain," 5th Edition, McGraw-Hill Book Company, 1975.
6. Fuchs, H.O., Stephens, R.I., "Metal Fatigue in Engineering," John Wiley & Sons, Inc., 1980.
7. Ferdinard P. Beer, E. Russel Johnston, Jr., "Mechanics of Materials," McGraw-Hill Book Company, 1981.
8. Findley, W.N., Mathur, P.N., Szczepanski, E., and Temel, A.O., "Energy versus Stress Theories for Combined Stress - A Fatigue Experiment Using a Rotating Disk," Trans. ASME 83(1), March, 10-14, 1961.
9. Stephen H. Crandall, Norman C. Dahl, and Thomas J. Lardner, "An Introduction to the Mechanics of Solids," 2nd Edition, McGraw-Hill Book Company, 1978.
10. R.A.C. Slater, "Engineering Plasticity (Theory and Application to Metal Forming Processes)," The Macmillan Press LTD, 1977.
11. Arturs Kalnins, Dean P. Updike, "Shakedown and Stress Range of Torishperical Heads under Cyclic Internal Pressure," 1996 ASME/PVP vol. 339, pp. 25-31.
12. "ABAQUS/standard User's Manual Volume I & II," Hibbitt, Karlsson & Sorensen, Inc., 1993.
13. B. F. Langer, "Design of Pressure Vessels for Low-cycle Fatigue," Trans. ASME, September, 389-402, 1962.
14. ASME B&PV Code, 1995, Section VIII - Division 2, "Appendix 5 - Mandatory Design Based on Fatigue Analysis," American Society of Mechanical Engineers, NY.

15. Arturs Kalnins, "Stress analysis of Beams, Plates, and Shells," Class Notes, Lehigh University, 1984.
16. S. Timoshenko, S. Woinowsky-krieger, "Theory of Plates and Shells," 2nd Edition, McGraw-Hill Book Company, 1959.
17. Robert D. Cook, David S. Malkus, Michael E. Plesha, "Concepts and Applications of Finite Element Analysis," 3rd Edition, John Wiley & Sons, Inc., 1989.
18. John F. Harvey, "Theory and Design of Modern Pressure Vessels," 2nd Edition, Van Nostrand Reinhold Company, 1974.
19. E. C. Rodabaugh, "A Review of Area Replacement Rules for Pipe Connections in Pressure Vessels and Piping," Welding Research Council, ISSN 0043-2326, August 1988.
20. Arturs Kalnins, Dean P. Updike, and Ingyu Park, "Plastic straining at Nozzles in Pressure Vessels," submitted to 1997 ASME/PVP conference.

Vita

December 31, 1961	Born in Taegu, Korea
August 31, 1988	B.S., Yeungnam University Kyongsan, Korea
September 6, 1988 ~ August 15, 1995	Engineer, Hyundai Motor Company
August 1995 ~ June 1997	Graduate Student, Lehigh University Supported by Hyundai Motor Company
August 1997	Engineer, Hyundai Motor Company

END OF TITLE